

Hypervulnerability to sound-exposure through impaired adaptive proliferation of peroxisomes

Sedigheh Delmaghani^{1,2,3}, Jean Defourny^{1,2,3}, Asadollah Aghaie^{2,3,4}, Maryline Beurg⁵, Didier Dulon⁵, Nicolas Thelen⁶, Isabelle Perfettini^{1,2,3}, Tibor Zelles^{7,8}, Mate Aller⁷, Anaïs Meyer^{1,2,3}, Alice Emptoz^{1,2,3}, Fabrice Giraudet^{9,10,11}, Michel Leibovici¹², Sylvie Dartevelle¹³, Marc Thiry⁶, E. Sylvester Vizi⁷, Saaïd Safieddine^{1,2,3}, Jean-Pierre Hardelin^{1,2,3}, Paul Avan^{9,10,11,15} and Christine Petit^{1,2,3,4,14,15,*}

¹Unité de Génétique et Physiologie de l'Audition, Institut Pasteur, 75015 Paris, France

²UMRS 1120, Institut National de la Santé et de la Recherche Médicale (INSERM), 75015 Paris, France

³Sorbonne Universités, UPMC Université Paris 06, Complexité du Vivant, 75005 Paris, France

⁴Syndrome de Usher et Autres Atteintes Rétino-Cochléaires, Institut de la Vision, 75012 Paris, France

⁵Equipe Neurophysiologie de la Synapse Auditiv, Université Victor Segalen and Bordeaux Neurosciences Institute, CHU Pellegrin, 33076 Bordeaux, France

⁶Unit of Cell and Tissue Biology, GIGA-Neurosciences, University of Liege, CHU Sart-Tilman, B36, 4000 Liege, Belgium

⁷Institute of Experimental Medicine, Hungarian Academy of Sciences, Budapest, Hungary

⁸Department of Pharmacology and Pharmacotherapy, Semmelweis University, Budapest, Hungary

⁹Laboratoire de Biophysique Sensorielle, Université d'Auvergne, 63000 Clermont-Ferrand, France

¹⁰UMR 1107, Institut National de la Santé et de la Recherche Médicale (INSERM), Clermont-Ferrand, France

¹¹Centre Jean Perrin, 63000 Clermont-Ferrand, France

¹²UMR 8104, Institut Cochin, 75014 Paris, France

¹³Plateforme d'Ingénierie des Anticorps, Institut Pasteur, 75015 Paris, France

¹⁴Collège de France, 75005 Paris, France

1
2 ¹⁵Co-senior author

3
4 *Correspondence: christine.petit@pasteur.fr
5

6 **SUMMARY :**

7 **A deficiency of pejvakin, a protein of unknown function, causes a strikingly**
8 **heterogeneous form of deafness. Pejvakin-deficient (*Pjvk*^{-/-}) mice also exhibited variable**
9 **phenotypes. Correlation between their hearing thresholds and the number of pups per**
10 **cage suggested a possible harmful effect of pup vocalizations. Direct sound or electrical**
11 **stimulation showed that the cochlear sensory hair cells and auditory pathway neurons**
12 **of *Pjvk*^{-/-} mice and patients were exceptionally vulnerable to sound. *Pjvk*^{-/-} cochleas**
13 **displayed features of marked oxidative stress and impaired anti-oxidant defenses. We**
14 **showed that pejvakin is associated with peroxisomes, and is required for the oxidative**
15 **stress-induced proliferation of these organelles. In *Pjvk*^{-/-} hair cells, peroxisomes**
16 **displayed structural abnormalities after the onset of hearing. Noise-exposure of wild-**
17 **type mice rapidly upregulated *Pjvk* cochlear transcription, and triggered peroxisome**
18 **proliferation in hair cells and primary auditory neurons. Our results reveal that the**
19 **anti-oxidant activity of peroxisomes protects the auditory system against noise-induced**
20 **damage.**

21
22 **HIGHLIGHTS**

23
24 Pejvakin-deficient mice and humans are hypervulnerable to sound exposure.

25
26 Oxidative stress induces a pejvakin-dependent proliferation of peroxisomes.

27 Peroxisome proliferation contributes to the physiological response to sound exposure.

28 *Pjvk* gene transfer can rescue *Pjvk*^{-/-} mice from auditory dysfunction.
29

1 INTRODUCTION

2 Mutations of *PJVK*, which encodes pejvakin, a protein of unknown function present
3 only in vertebrates, cause the DFNB59 recessive form of sensorineural hearing impairment.
4 In the first patients described (Delmaghani et al., 2006), the impairment was restricted to
5 neurons of the auditory pathway, as demonstrated by the combination of abnormal auditory
6 brainstem responses (ABRs) with decreased wave amplitudes and increased inter-wave
7 latencies (Starr & Rance, 2015). ABRs monitor the electrical response of auditory pathways
8 to brief sound stimuli, from the primary auditory neurons synapsing with the sensory cells of
9 the cochlea, the inner hair cells (IHCs), to the colliculus in the midbrain (Møller & Jannetta,
10 1983). However, some DFNB59 patients were found to have a cochlear dysfunction, as
11 shown by an absence of the otoacoustic emissions (OAEs) that are produced by the outer
12 hair cells (OHCs), frequency-tuned cells endowed with electromotility that mechanically
13 amplify the sound-stimulation of neighboring IHCs (Ashmore, 2008). These patients had
14 truncating mutations of *PJVK*, whereas the previously identified patients had missense
15 mutations (p.T54I or p.R183W) (Ebermann et al., 2007; Schwander et al., 2007; Borck et
16 al., 2011). However, the identification of patients also carrying the p.R183W missense
17 mutation but lacking OAEs (Collin et al., 2007) refuted any straightforward connection
18 between the nature of the *PJVK* mutation and the hearing phenotype. The severity of
19 deafness in DFNB59 patients varies from moderate to profound, and may even be
20 progressive in some patients, suggesting that extrinsic factors may influence the hearing
21 phenotype.

22 We investigated the role of pejvakin, with the aim of determining the origin of the
23 phenotypic variability of the DFNB59 form of deafness. Our study of *Pjvk* knockout mouse
24 models and of patients revealed an unprecedented hypervulnerability of auditory hair cells
25 and neurons to sound-exposure, accounting for phenotypic variability. We found that

1 pejvakin is a peroxisome-associated protein involved in the oxidative stress-induced
2 proliferation of this organelle. Pejvakin-deficient mice revealed the key role of peroxisomes
3 in the redox homeostasis of the auditory system and in the protection against noise-induced
4 hearing loss.

5

6 **RESULTS**

7 **Heterogeneity in the hearing sensitivity of *Pjvk*^{-/-} mice**

8 We generated pejvakin-null (*Pjvk*^{-/-}) mice carrying a deletion of *Pjvk* exon 2 resulting
9 in a frameshift at codon position 71 (p.Gly71fs*9) (Figure S1 and see Extended
10 Experimental Procedures). ABRs were recorded on postnatal day 30 (P30), to assess hearing
11 sensitivity. ABR thresholds at 10 kHz ranged from 35 to 110 dB SPL in these mice (n = 48),
12 but never exceeded 30 dB SPL in their *Pjvk*^{+/+} littermates (n = 26) (Figure 1A). This broad
13 range of hearing sensitivity in *Pjvk*^{-/-} mice, from near-normal hearing to almost complete
14 deafness, extended across the whole frequency spectrum. The thresholds of distortion-
15 product OAEs (DPOAEs) at 10 kHz (i.e. the minimum stimulus required for DPOAEs
16 production by OHCs) also fell within an abnormally large range of values, from 30 to 75 dB
17 SPL, in 28 *Pjvk*^{-/-} mice, corresponding to OHC dysfunction, and DPOAEs were undetectable
18 in another 20 *Pjvk*^{-/-} mice, indicating a complete OHC defect (Figure 1B). The absence of
19 pejvakin in mice thus results in a puzzlingly large degree of hearing phenotype variability.

20

21 **Hypervulnerability to the natural acoustic environment in *Pjvk*^{-/-} mice**

22 We investigated the variability of *Pjvk*^{-/-} auditory phenotypes, by first determining
23 the ABR thresholds of *Pjvk*^{-/-} littermates from different crosses. Large differences were
24 observed between crosses, with much lesser differences between the *Pjvk*^{-/-} littermates of
25 individual crosses. Litters with larger numbers of pups (6 to 12) had higher ABR thresholds,

1 suggesting that the natural acoustic environment, with the calls of larger numbers of pups,
2 might be deleterious in *Pjvk*^{-/-} mice. Pups are vocally very active from birth to about P20.
3 We manipulated the level of exposure to pup calls by randomly splitting large litters of *Pjvk*^{-/-}
4 pups into groups of 2, 4, 6 and 10 pups per cage, with foster mothers, before the onset of
5 hearing (P10). The ABR thresholds at P21 were significantly correlated with the number of
6 pups raised together ($p < 0.001$, $r^2 = 0.51$, i.e. 51% of the variation in ABR threshold is
7 determined by the number of pups per cage) (Figure 1C).

8 We then evaluated the effect on hearing of a controlled sound-stimulation, by
9 presenting 1000 tone bursts at 10 kHz, 105 dB SPL (2-ms plateau stimulations separated by
10 60-ms intervals of silence), energetically equivalent to a 3-minute stay in the natural
11 environment of a 12-pup litter, while monitoring the ABRs during sound-exposure. These
12 conditions are referred to hereafter as "controlled sound-exposure". We probed the effect of
13 sound exposure by ABR tests which, limited to 50 repetitions of tone bursts, did not
14 influence the hearing thresholds of *Pjvk*^{-/-} mice. In a sample of P30 *Pjvk*^{-/-} mice with initial
15 ABR threshold elevation below 35 dB SPL, controlled sound-exposure affected ABR
16 thresholds in the 12-20 kHz frequency interval (corresponding to the cochlear zones where
17 hair-cell stimulation was strongest (Cody & Johnstone, 1981)), with an immediate increase
18 of 21.7 ± 10.3 dB ($n = 8$; $p < 0.001$), not observed in *Pjvk*^{+/+} mice (2.2 ± 2.4 dB, $n = 12$; $p =$
19 0.3) (Figure 1D). *Pjvk*^{-/-} mice transferred to a silent environment after exposure displayed a
20 further increase of 33.7 ± 16.0 dB ($n = 8$) two days after exposure. The threshold shift
21 decreased to 23.7 ± 18.0 dB at seven days, and disappeared entirely by 14 days. When
22 exposed mice were returned to the box with their littermates, their ABR continued to
23 increase, at a rate of 15 dB per week. *Pejvakin* deficiency thus results in particularly high
24 levels of vulnerability to low levels of acoustic energy, and the increase in ABR thresholds
25 is reversible but only slowly and in a quiet environment.

1

2 **Hair cells and auditory pathway neurons are affected by pejvakin deficiency**

3 To identify the cellular targets of the pejvakin deficiency, we specifically probed the
4 function of auditory hair cells and neurons in *Pjvk*^{-/-}, hair cell-conditional *Pjvk* knockout
5 (*Pjvk*^{fl/fl}*Myo15-cre*^{-/-}), and *Pjvk*^{+/+} mice, at the age of three weeks, before and after controlled
6 sound-exposure or controlled electrical simulation. The responses of the IHCs to sound-
7 induced vibrations amplified by OHCs trigger action potentials in the distal part of primary
8 auditory neurons, at the origin of ABR wave-I. In *Pjvk*^{fl/fl}*Myo15-cre*^{+/-} mice, which lack
9 pejvakin only in the hair cells, ABR wave-I amplitude and latency at 105 dB SPL
10 specifically probed IHC function, because IHC responses to such loud sounds are
11 independent of OHC activity (Robles & Ruggero, 2001). The larger wave-I latency (1.58 ms
12 in *Pjvk*^{fl/fl}*Myo15-cre*^{+/-} mice (n = 20) vs. 1.32 ms in *Pjvk*^{+/+} littermates (n = 30); p < 0.001)
13 and lower wave-I amplitude (37% of the amplitude in *Pjvk*^{+/+} littermates; p < 0.001)
14 suggested a dysfunction of the IHCs in the absence of pejvakin. Controlled sound exposure
15 induced further decreases in ABR wave-I amplitude in *Pjvk*^{-/-} and *Pjvk*^{fl/fl}*Myo15-cre*^{+/-} mice
16 (48% and 55% of pre-exposure amplitude, respectively) with respect to *Pjvk*^{+/+} mice (108%;
17 p < 0.001 for both comparisons) (Figure 2A), demonstrating that IHCs lacking pejvakin are
18 hypervulnerable to sound. As shown above, OHCs are also affected by the pejvakin
19 deficiency. Controlled sound-exposure triggered a mean increase in the DPOAE threshold of
20 17.1 ± 6.7 dB in the 12 to 20 kHz frequency interval (p < 0.0001) in *Pjvk*^{-/-} mice with
21 persistent DPOAEs (n = 8), but had no effect on the DPOAEs of *Pjvk*^{+/+} mice (n = 9; p =
22 0.51) (Figure 2B). OHCs lacking pejvakin are, thus, also hypervulnerable to sound.

23 We investigated the effect of the absence of pejvakin on the auditory pathway by
24 comparing electrically evoked brainstem responses (EEBR) in *Pjvk*^{-/-} and *Pjvk*^{fl/fl}*Myo15-*
25 *cre*^{+/-} mice (see Extended Experimental Procedures). The amplitudes of the most distinctive

1 EEER waves, E II and E IV, did not differ between the two types of mice (e.g., for wave E
2 IV: $2.6 \pm 1.8 \mu\text{V}$ in *Pjvk*^{-/-} mice (n = 18) and $2.2 \pm 1.2 \mu\text{V}$ in *Pjvk*^{fl/fl}*Myo15-cre*^{+/-} mice (n =
3 11); t-test, p = 0.13). However, following controlled electrical exposure at 200 impulses / s
4 for 1 minute, as opposed to electric-impulse stimulation with 16 impulses / s for 10 s for pre-
5 and post-exposure EEER tests, the amplitudes of the E II and E IV EEER waves were 41%
6 and 47% smaller, respectively, for at least 3 minutes, in *Pjvk*^{-/-} mice (n = 5; p = 0.02 and p =
7 0.01, respectively), but were unaffected in *Pjvk*^{fl/fl}*Myo15-cre*^{+/-} mice (n = 10) (Figures 2D,
8 2G-2I). The E II-E IV interwave interval was 0.41 ms longer in *Pjvk*^{-/-} mice (n = 5) than in
9 *Pjvk*^{fl/fl}*Myo15-cre*^{+/-} mice (n = 10; t-test; p = 0.003) and controlled electrical exposure
10 extended this interval by a further 0.15 ms in *Pjvk*^{-/-} mice only (paired t-test, p = 0.001)
11 (Figures 2H and 2I). Likewise, the latency interval between ABR wave I and wave IV (the
12 counterpart of wave E IV) was abnormal in one third of the *Pjvk*^{-/-} mice tested (n = 12)
13 (Figures 2C and 2E), and was further increased by controlled sound-exposure in all *Pjvk*^{-/-}
14 mice (n = 12 ears with an ABR threshold < 95 dB SPL, a mean increase of 0.16 ms relative
15 to the pre-exposure value; paired t-test, p < 0.001). By contrast, it remained normal in
16 *Pjvk*^{fl/fl}*Myo15-cre*^{+/-} mice (n = 10 ears; p = 0.73) (Figures 2C and 2F). We conclude that the
17 absence of pejkakin affects the propagation of action potentials in the auditory pathway after
18 both controlled electrical and sound-exposure, as demonstrated by the reduced amplitude of
19 the E II wave and the increased E II-E IV and ABR I-IV interwave intervals in *Pjvk*^{-/-} mice.

20 We tested whether these abnormalities were of neuronal or glial origin by performing
21 a rescue experiment in *Pjvk*^{-/-} mice, using adeno-associated virus 8 (AAV8) vector-mediated
22 transfer of the murine pejkakin cDNA. AAV8 injected into the cochlea transduces the
23 primary auditory neurons and neurons of the cochlear nucleus (Figure S2A). All *Pjvk*^{-/-} mice
24 (n = 7) injected on P3 and tested on P21 had normal ABR interwave I-IV latencies (Figure
25 2J), and their EEER wave-E IV amplitude was insensitive to controlled electrical

1 stimulation ($1.91 \pm 0.97 \mu\text{V}$ before and $1.87 \mu\text{V} \pm 1.07$ after stimulation; paired t-test, $p =$
2 0.59) (Figures 2K and 2L). The absence of pejvakin thus renders auditory pathway neurons
3 hypervulnerable to exposure to mild, short stimuli.

4

5 **Hypervulnerability to sound in DFNB59 patients**

6 We then investigated whether the hearing of DFNB59 patients was also
7 hypervulnerable to sound-exposure. We tested five patients carrying the p.T54I mutation
8 from the series reported by Delmaghani et al. (2006). Transient-evoked OAEs (TEOAEs)
9 assessing OHC function over a broad range of frequencies were detected for all ears, despite
10 the severe hearing impairment (hearing threshold increasing from 66 dB HL at 250 Hz to 84
11 dB at 8 kHz). Following minimal exposure to impulse stimuli (clicks at 99 dB nHL), ABR
12 waves were clearly identified in response to 250 clicks. When exposure was prolonged to
13 1000 clicks (the standard procedure), wave V, the equivalent of mouse ABR-wave IV, which
14 was initially conspicuous, displayed a marked decrease in amplitude (to $39 \pm 30\%$ of its
15 initial amplitude) and an increase in latency (of 0.30 ± 0.15 ms) (Figure 3A, 3C, and 3D). In
16 parallel, the I-V interwave interval increased by 0.30 ± 0.15 ms. Wave-V amplitude and
17 latency recovered fully after 10 minutes of silence (Figure 3B). In control patients with
18 sensorineural hearing impairment of cochlear origin matched for ABR thresholds, similar
19 sound stimulation did not affect ABR wave-V amplitude ($105 \pm 14\%$ of the initial amplitude
20 after exposure; $n = 13$ patients) or latency (-0.02 ± 0.07 ms change after exposure) (Figures
21 3C and 3D). Exposure of the DFNB59 patients to 1000 clicks also affected TEOAEs ($6.1 \pm$
22 5.2 dB nHL decrease in amplitude; paired t-test, $p = 0.02$). Therefore, as in pejvakin-
23 deficient mice, the cochlear and neuronal responses of DFNB59 patients were affected by
24 exposure to low-energy sound.

25

1 **Redox status abnormalities and ROS-induced cell damage in the cochlea of *Pjvk*^{-/-} mice**

2 We investigated the impact of pejvakin deficiency on cochlear structure in *Pjvk*^{-/-} mice,
3 by light microscopy on semithin sections, and electron microscopy. On P15 and P21, both
4 OHCs and IHCs were normal in number and shape. Their hair bundles (the
5 mechanoreceptive structures responding to sound), the ribbon synapses of the IHCs and their
6 primary auditory neurons were unmodified (data not shown). On P30, we observed the loss
7 of a few OHCs (16 %), restricted to the basal region of the cochlea (tuned to high-frequency
8 sounds). From P30 onwards, numerous OHCs and cochlear ganglion neurons disappeared
9 and the sensory epithelium (organ of Corti) progressively degenerated (Figure S3A).

10 We investigated possible changes in gene expression in the organ of Corti (which
11 includes not only hair cells, but also various types of supporting cells) in young *Pjvk*^{-/-} mice,
12 by microarray studies on P15 (see Extended Experimental Procedures). Eighteen genes had
13 expression levels at least 1.5-fold higher or lower in *Pjvk*^{-/-} mice than in *Pjvk*^{+/+} mice.
14 Marked differences were observed for four genes involved in the redox balance — *CypA*,
15 *Gpx2*, *c-Dct*, and *Mpv17* — encoding cyclophilin A, glutathione peroxidase 2, c-
16 dopachrome tautomerase, and Mpv17, respectively (Table S1). All these genes were
17 downregulated in *Pjvk*^{-/-} mice, a result confirmed by quantitative RT-PCR (Figure S4A), and
18 all encode antioxidant proteins, suggesting an impairment of antioxidant defenses in *Pjvk*^{-/-}
19 mice (Table S1).

20 We thus assessed anti-oxidant defenses in the cochlea of P21 *Pjvk*^{-/-} mice, by
21 determining the ratio of reduced to oxidized glutathione (GSH:GSSG). The GSSG content
22 was about three times larger than in *Pjvk*^{+/+} mice, whereas the GSH content was 23%
23 smaller, resulting in a GSH:GSSG ratio in *Pjvk*^{-/-} cochleas lower than that in *Pjvk*^{+/+} cochleas
24 by a factor of 3.4 (Figure 4A). No significant differences in GSSG and GSH levels or in the
25 GSH:GSSG ratio in the liver were detected between *Pjvk*^{+/+} and *Pjvk*^{-/-} mice (data not

1 shown). Increase in GSSG level and decrease in the GSH:GSSG ratio are markers of the
2 cochlear oxidative stress accompanying the pejvakin deficit.

3 We assessed lipid peroxidation by reactive oxygen species (ROS) in *Pjvk*^{-/-} mice, by
4 immunofluorescence-based detection of the by-product 4-hydroxy-2-nonenal (4-HNE).
5 Strong immunoreactivity was observed in P60 *Pjvk*^{-/-} hair cells and cochlear ganglion
6 neurons (Figure S3B). Quantification of lipid peroxidation in microdissected organs of Corti
7 from P30 *Pjvk*^{-/-} and *Pjvk*^{+/+} mice, showed a moderate (16%) but statistically significant
8 increase of the malondialdehyde content in the absence of pejvakin ($2.15 \pm 0.14 \mu\text{M}$ in *Pjvk*
9 ^{-/-} vs. $1.84 \pm 0.11 \mu\text{M}$ in *Pjvk*^{+/+} mice, means \pm SD; t-test, $p = 0.04$). Thus, pejvakin
10 deficiency led to impaired antioxidant defenses in the cochlea, resulting in ROS-induced cell
11 damage.

12 We then studied electrophysiological features of IHCs and OHCs in the mature
13 cochlea of P19-P21 *Pjvk*^{-/-} mice. In IHCs, the number of synaptic ribbons, Ca^{2+} currents, and
14 synaptic exocytosis (assessed by monitoring the increase of the cell capacitance following
15 cell depolarization) were unaffected (Figure S7A). As IHC functions also depend on
16 potassium ion channels known to be affected by ROS, we investigated whether *Pjvk*^{-/-} mice
17 display the main K^+ currents found in mature IHCs, specifically $I_{\text{K},\text{f}}$, which plays a major
18 part in IHC repolarization and is involved in the high temporal precision of action potentials
19 in postsynaptic nerve fibers, $I_{\text{K},\text{s}}$, and $I_{\text{K},\text{n}}$ (Oliver et al., 2006). In *Pjvk*^{-/-} mice, $I_{\text{K},\text{f}}$ flowing
20 through the large conductance voltage- and Ca^{2+} -activated potassium (BK) channels, a
21 known target of ROS (Tang et al., 2004), was detected in only 4 out of 11 *Pjvk*^{-/-} IHCs, and
22 the mean number of spots immunolabeled for the BK α -subunit per IHC was much lower in
23 *Pjvk*^{-/-} mice (5.0 ± 1.4 , $n = 283$ IHCs from 7 mice) than in *Pjvk*^{+/+} mice (13.9 ± 2.6 , $n = 204$
24 IHCs from 9 mice; t-test, $p < 0.001$). By contrast, the $I_{\text{K},\text{s}}$ and $I_{\text{K},\text{n}}$ currents were not affected
25 (Figure 4B and Figure S7B). The electromotility of OHCs was also impaired in P19-P21

1 *Pjvk*^{-/-} mice, as shown by the reduction of the non-linear cell capacitance, the electrical
2 correlate of electromotility (Ashmore, 2008) (Figure S7C). Moreover, the total loss of
3 DPOAE in a large majority of *Pjvk*^{-/-} mice from P15 on, even at the highest possible stimulus
4 level of 75 dB SPL, pinpointed a major additional defect of the mechano-electrical
5 transduction in OHCs, the main determinant of DPOAEs at high stimulus levels when OHC
6 electromotility, which amplifies cochlear vibrations at low levels, bears minimal influence
7 on DPOAE production (Avan et al., 2013). Measurements of the cochlear microphonic
8 potential at the round window, a far-field electric potential oscillating at the stimulus
9 frequency that reflects mechano-electrical transduction currents through OHCs of the basal-
10 most cochlear region, indeed corroborated the DPOAE measurements: this potential,
11 recorded for a 5 kHz sound stimulus at 95 dB SPL, was always larger than 10 μ V in *Pjvk*^{+/+}
12 mice (n = 8), but fell between 3 μ V and 5 μ V in the P21 *Pjvk*^{-/-} mice that displayed residual
13 DPOAEs (n = 2), and was below 1 μ V, indistinguishable from electric artefacts, in the
14 mutants that had lost their DPOAEs (n = 6). Taken together, these results allowed us to
15 conclude that the impaired antioxidant defenses in the *Pjvk*^{-/-} cochlea have an impact on
16 various electrophysiological properties of the hair cells, particularly mechanotransduction
17 and K⁺ current through BK channels.

18 Even though mitochondrial defects are a common cause of ROS overproduction, we
19 didn't find evidence that mitochondria were damaged, as vulnerability of the mitochondrial
20 membrane potential, $\Delta\psi_m$, to the uncoupler carbonyl cyanide 4-
21 (trifluoromethoxy)phenylhydrazone (FCCP) in the organ of Corti and cochlear ganglion was
22 similar in P17-P30 *Pjvk*^{-/-} and *Pjvk*^{+/+} mice, and transmission electron microscopy of *Pjvk*^{-/-}
23 hair cells revealed no mitochondrial abnormalities (Figure S7D and data not shown).

24

25 **Pejvakin is a peroxisome-associated protein**

1 By using *Pjvk*^{-/-} cochlea as control, we found that neither the commercially available
2 antibodies nor our initial polyclonal antibody (Delmaghani et al., 2006) specifically
3 recognized pejvakin (data not shown). Given the limited divergence of the pejvakin amino-
4 acid sequence among vertebrates (97% sequence identity between mice and humans), we
5 tried to elicit an immune response in *Pjvk*^{-/-} mice (see Experimental Procedures). The
6 monoclonal antibody obtained, Pjvk-G21, yielded punctate immunostaining throughout the
7 cytoplasm of transfected HeLa cells expressing pejvakin, whereas no such staining was
8 observed in non-transfected cells. Double staining for peroxisome membrane protein 70
9 (PMP70) demonstrated the colocalization of pejvakin and peroxisomes (Figure S5A). In the
10 human HepG2 hepatoblastoma cell line, which is particularly rich in peroxisomes, strong
11 immunolabeling for endogenous pejvakin was associated with the peroxisomes (Figure 5A).
12 Finally, the specificity of the Pjvk-G21 antibody was demonstrated by the immunoreactivity
13 of peroxisomes in the hair cells of *Pjvk*^{+/+}, but not *Pjvk*^{-/-} mice (Figure 5B and S5B).

14 Peroxisomal matrix proteins are imported into the peroxisome by interaction with
15 peroxin 5 or peroxin 7, via the PTS1 or PTS2 targeting signals (Smith and Aitchison, 2013).
16 Prediction programs identified no PTS1 or PTS2 motifs in the pejvakin sequence (Mizuno
17 et al., 2008), suggesting that pejvakin is a peroxisomal membrane or membrane-associated
18 protein.

19

20 **Ultrastructural abnormalities of peroxisomes in the hair cells of *Pjvk*^{-/-} mice**

21 We investigated the distribution and morphology of peroxisomes in the *Pjvk*^{-/-}
22 cochlea by transmission electron microscopy. Peroxisomes were identified on the basis of
23 catalase activity detection using 3,3'-diaminobenzidine as substrate. We focused on OHCs,
24 the first to display a dysfunction in the mutant mice. On P30 but not P15, both the
25 distribution and shape of peroxisomes differed between *Pjvk*^{-/-} and *Pjvk*^{+/+} mice (Figure 5E).

1 In *Pjvk*^{+/+} mice, the peroxisomes were restricted to an area immediately below the cuticular
2 plate, a meshwork of actin filaments under the apical surface of the hair cells. In *Pjvk*^{-/-} mice,
3 the peroxisomes located just below the cuticular plate were slightly larger than those in
4 *Pjvk*^{+/+} mice. Strikingly, irregular catalase-containing structures, some of which were
5 juxtaposed, were present in the perinuclear region, at the immediate vicinity of the nuclear
6 membrane, of all *Pjvk*^{-/-} OHCs, but not of *Pjvk*^{+/+} OHCs, which never contained any
7 peroxisome either at this emplacement (Figure 5E). The lack of pejvakin thus results in
8 peroxisome abnormalities in cochlear OHCs after the onset of hearing.

9

10 **Pejvakin is involved in oxidative stress-induced peroxisome proliferation**

11 In HepG2 cells, protrusions emerging from some peroxisomes, the first step of
12 peroxisome biogenesis from pre-existing peroxisomes, were immunoreactive for pejvakin.
13 String-of-beads structures corresponding to elongated and constricted peroxisomes,
14 preceding final fission (Smith and Aitchison, 2013), were also pejvakin-immunoreactive,
15 suggesting a role of this protein in peroxisome proliferation (Figure S5C). Peroxisomes
16 actively contribute to cellular redox balance, by producing and scavenging/degrading H₂O₂
17 through a broad spectrum of oxidases and peroxidases (especially catalase), respectively
18 (Schrader and Fahimi, 2006). Because *Pjvk*^{-/-} mice displayed features of marked oxidative
19 stress in the cochlea, we investigated the possible role of pejvakin in peroxisome
20 proliferation in response to oxidative stress induced by H₂O₂, which upregulates the
21 expression of peroxisome biogenesis genes (Lopez-Huertas et al., 2000). Embryonic
22 fibroblasts derived from *Pjvk*^{+/+} and *Pjvk*^{-/-} mice were exposed to 0.5 mM H₂O₂ for 4 hours,
23 and cells were analyzed after 18 hours of incubation in H₂O₂-free culture medium (see
24 Experimental Procedures). In unexposed cells, the number of peroxisomes was similar
25 between the two genotypes (t-test, p = 0.82). After H₂O₂ treatment, the number of

1 peroxisomes was increased by 46% in *Pjvk*^{+/+} fibroblasts (p = 0.004) but remained
2 unchanged in *Pjvk*^{-/-} fibroblasts (p = 0.83), resulting in a statistically significant difference
3 between the two genotypes (p < 0.001) (Figures 5C and S6A).

4 We then asked whether mutations reported in DFNB9 patients also affect peroxisome
5 proliferation. To this purpose, we assessed the number of peroxisomes in transfected HeLa
6 cells producing EGFP alone, EGFP and murine pejvakin, or EGFP and one of the mutated
7 forms of murine pejvakin carrying the mutations responsible for DFNB59 (p.T54I,
8 p.R183W, p.C343S, or p.V330Lfs*7). Cells producing the non-mutated pejvakin had larger
9 numbers of peroxisomes than cells producing EGFP alone, whereas cells producing any of
10 the mutated forms of pejvakin (mutPjvk-IRES-EGFP) had smaller peroxisome numbers. In
11 addition, many of these cells contained enlarged peroxisomes, a feature typical of
12 peroxisome proliferation disorders (Ebberink et al., 2012) (Figure 5D and S6B). Together,
13 these results strongly suggest that pejvakin is directly involved in the production of new
14 peroxisomes from pre-existing peroxisomes.

15

16 **Upregulation of *Pjvk* cochlear transcription and peroxisome proliferation in response** 17 **to sound**

18 We then asked whether pejvakin is involved in the physiological response to sound.
19 We first assessed the transcription of *Pjvk*, and of *CypA*, *Gpx2*, *c-Dct*, and *Mpv17* that were
20 downregulated in *Pjvk*^{-/-} mice, in microdissected organs of Corti from P21 wild-type mice,
21 with or without prior sound-stimulation (5-20 kHz, 105 dB SPL for 1 hour; see Extended
22 Experimental Procedures). Transcript levels were analyzed by quantitative RT-PCR at
23 various times (1, 3, 6, and 18 hours) after sound-exposure (Figure 6A). *Pjvk* transcript levels
24 had increased by factors of 1.9 ± 0.1 and 3.5 ± 0.7 after 1 hour and 6 hours, respectively.
25 *CypA*, *c-Dct* and *Mpv17* were also upregulated after 6 hours (by factors of 6.6 ± 1.2 , $4.3 \pm$

1 0.6 and 1.5 ± 0.1 , respectively), as were *c-Fos* and *Hsp70*, used as a positive control, but
2 *Gpx2* was not. Thus, noise-exposure elicits an upregulation of the transcription of *Pjvk* and
3 of genes downregulated in *Pjvk*^{-/-} mice and this effect is dependent on acoustic energy level
4 (Figure S4B).

5 Based on this result, we predicted that sound-exposure would lead to peroxisome
6 proliferation in the auditory system of wild-type mice. Six hours after exposure (5-20 kHz,
7 105 dB SPL for 1 hour), the numbers of peroxisomes were unchanged (34.5 ± 0.8 and 35.9
8 ± 1.0 per IHC from unexposed and sound-exposed mice, respectively, $n = 75$ cells from 6
9 mice, respectively; t-test, $p = 0.25$). However, at 48 hours, they had markedly increased, by
10 a factor of 2.3, in both IHCs and OHCs (84.7 ± 5.0 per IHC and 16.5 ± 1.0 per OHC, $n = 90$
11 cells and $n = 150$ cells from 6 mice, respectively) compared to unexposed mice (36.8 ± 3.0
12 per IHC and 7.3 ± 0.4 per OHC, $n = 90$ cells and $n = 150$ cells from 6 mice, respectively; t-
13 test, $p < 0.0001$ for both comparisons). The number of peroxisomes had also increased, by
14 35%, in the dendrites of primary auditory neurons (1.7 ± 0.1 and 2.3 ± 0.2 peroxisomes per
15 μm of neurite length, $n = 40$ neurites from 5 unexposed and 5 sound-exposed *Pjvk*^{+/+} mice,
16 respectively; t-test, $p = 0.003$).

17

18 **Therapeutic approaches in *Pjvk*^{-/-} mice**

19 We used the classical anti-oxidant drug N-acetyl cysteine (either alone or associated
20 with α -lipoic acid and α -tocopherol; see Experimental procedures), which was administered
21 to *Pjvk*^{-/-} pups. The ABR thresholds of P21 *Pjvk*^{-/-} pups treated with N-acetyl cysteine alone
22 ($n = 21$) were about 10 dB lower than those of untreated *Pjvk*^{-/-} pups ($n = 24$) for all
23 frequencies tested (10, 15, 20, and 32 kHz; t-test, $p < 0.001$ for all comparisons) (Figure
24 7A). N-acetyl cysteine principally affected the amplitude of the ABR wave I elicited at 105
25 dB SPL, which was similar to that in age-matched *Pjvk*^{+/+} mice and greater than that in

1 untreated *Pjvk*^{-/-} mice ($4.35 \pm 1.16 \mu\text{V}$, n = 21; $4.36 \pm 1.15 \mu\text{V}$, n = 18; and $1.88 \pm 1.07 \mu\text{V}$, n
2 = 24, respectively; ANOVA, p < 0.001) (Figure 7B). EEBRs were more resistant to the
3 high-rate electrical stimulation in treated than in untreated mutant mice (Figure 7C).
4 Conversely, N-acetyl cysteine had no beneficial effect on OHCs (data not shown). The
5 association of N-acetyl cysteine with α -lipoic acid and α -tocopherol did not perform any
6 better (data not shown).

7 Full recovery of the neuronal phenotype was achieved by the intracochlear injection
8 of AAV8-mediated pejkakin cDNA (see above). This viral vector does not transduce hair
9 cells, so OHCs remained non-functional (no detectable DPOAE, n = 9), and ABR wave-I
10 amplitude, which is controlled by IHC function, did not differ significantly between *Pjvk*^{-/-}
11 mice receiving AAV8 containing the pejkakin cDNA ($3.3 \pm 1.8 \mu\text{V}$, n = 9), the EGFP cDNA
12 only ($3.2 \pm 1.3 \mu\text{V}$, n = 5), or with no injection ($2.7 \pm 1.4 \mu\text{V}$, n = 11) (ANOVA, p = 0.54).
13 We thus investigated whether AAV2/8, which transduces hair cells only (Figure S2B), could
14 rescue the hair-cell phenotype in *Pjvk*^{-/-} mice. The auditory function of *Pjvk*^{-/-} mice (n = 7,
15 four pups per cage in every experiment) receiving intracochlear injections of AAV2/8-
16 pejkakin cDNA (Pjvk-IRES-EGFP) on P3 was assessed on P21, and the percentage of
17 transduced IHCs and OHCs was evaluated in each injected and contralateral cochlea, on the
18 basis of EGFP fluorescence. Improvements in ABR thresholds of 20 to 30 dB SPL with
19 respect to untreated mice were observed for frequencies between 10 and 20 kHz (t-test, p <
20 0.001 for all comparisons; Figure 7D). With the same vector expressing the EGFP cDNA
21 only (n = 6), ABR thresholds were similar to those of untreated *Pjvk*^{-/-} mice (n = 10) (81.6
22 vs. 78.6 dB SPL for 10 kHz, p = 0.64). A partial reversion of the OHC dysfunction was
23 obtained, with detectable DPOAEs in pejkakin cDNA-treated cochleas (threshold $54.0 \pm$
24 10.7 dB), but not in contralateral, untreated cochleas (Figure 7F). DPOAE thresholds were
25 linearly correlated ($r^2 = 0.74$, p < 0.001) with the number of EGFP-tagged OHCs (Figure

1 7G), suggesting that the normalization of DPOAE thresholds may be possible if all OHCs
2 could be transduced. The latency of the ABR wave I in response to a 105 dB SPL
3 stimulation decreased significantly (1.38 ± 0.11 ms vs. 1.53 ± 0.10 ms; *t*-test, $p = 0.026$)
4 (Figure 7E), and its amplitude increased into the normal range (7.34 ± 0.80 μ V for the
5 treated ears, $n = 6$, vs. 2.93 ± 0.92 μ V for the contralateral, untreated ears; paired *t*-test, $p <$
6 0.001) (Figure 7H), in relation to the number of EGFP-tagged IHCs ($r^2 = 0.89$ for wave I
7 amplitude, $p < 0.001$; Figure 7I). No correction of the interwave I-IV latency was observed,
8 as expected (data not shown).

9 Finally, we investigated the effect of the transduction of *Pjvk*^{-/-} IHCs by AAV2/8-
10 pejvakin cDNA on their peroxisomes. Before sound-exposure, the numbers of peroxisomes
11 in IHCs of *Pjvk*^{-/-} and AAV2/8-Pjvk *Pjvk*^{-/-} mice did not differ from that of *Pjvk*^{+/+} mice
12 (30.5 ± 1.9 , 32.3 ± 2.1 , and 36.8 ± 3.0 peroxisomes per IHC, $n = 60$ cells from 4 *Pjvk*^{-/-} and
13 4 AAV2/8-Pjvk *Pjvk*^{-/-} mice, and $n = 90$ cells from 6 *Pjvk*^{+/+} mice, respectively; respective *t*-
14 test, $p = 0.11$ and $p = 0.30$). By contrast, 48 hours after sound-exposure (5-20 kHz) at 105
15 dB SPL for 1 hour, the number of peroxisomes had decreased by 63% in *Pjvk*^{-/-} IHCs ($30.5 \pm$
16 1.9 and 11.2 ± 1.3 peroxisomes per IHC, $n = 75$ cells from 5 unexposed and 5 sound-
17 exposed *Pjvk*^{-/-} mice, respectively; *t*-test, $p < 0.0001$), and enlarged PMP70-labeled
18 structures were present close to the nucleus (Figure 7J). In response to the same sound but of
19 a lower intensity, i.e. 97 dB SPL for 1 hour, the number of peroxisomes was unchanged in
20 *Pjvk*^{-/-} IHCs (30.5 ± 1.9 and 34.6 ± 2.3 peroxisomes per IHC, $n = 60$ cells from 4 unexposed
21 and 4 sound-exposed *Pjvk*^{-/-} mice, respectively; *t*-test, $p = 0.17$), and no enlarged PMP70-
22 stained structures were detected (data not shown). Thus, depending on the acoustic energy of
23 the sound stimulation, in the absence of pejvakin, peroxisomes failed to proliferate in IHCs
24 (both at 105 dB SPL and 97 dB SPL), and even degenerated (at 105 dB SPL). In AAV2/8-
25 Pjvk injected *Pjvk*^{-/-} mice exposed to 105 dB SPL for 1 hour, enlarged PMP70-labeled

1 structures were no longer detected in transduced IHCs and the number of peroxisomes
2 increased by 35% (32.3 ± 2.1 and 43.7 ± 3.0 peroxisomes per IHC, $n = 60$ cells from
3 unexposed and exposed transduced *Pjvk*^{-/-} IHCs, respectively, t-test, $p = 0.002$) (Figure 7J).
4 We conclude that pejvakin re-expression fully protects *Pjvk*^{-/-} IHCs from peroxisome
5 degenerescence and partially restores their impaired adaptive proliferation.

6

7 **DISCUSSION**

8 Noise overexposure, a major threat to hearing, affects 15% of people between the
9 ages of 20 and 69 years. There are currently no efficient methods for curing noise-induced
10 hearing loss (NIHL), and we still know little about the underlying pathogenic processes. We
11 describe here a genetic form of NIHL, by showing that pejvakin deficiency in mice and
12 DFNB59 patients leads to hypervulnerability to sound, due to a peroxisomal deficiency.
13 This is the first reported peroxisomal cause of an isolated (non-syndromic) form of inherited
14 deafness. The peroxisome emerges as a key organelle in the redox homeostasis of the
15 auditory system, for coping with the overproduction of ROS induced by high levels of
16 acoustic energy.

17 Acoustic energy is the main determinant of NIHL. The $L_{EX,8 \text{ hour}}$ (for level of
18 exposure over an 8-hour workshift) index has been defined such that an $L_{EX,8 \text{ hour}}$ of X dB
19 delivers the same energy as a stable sound of X dB played over a period of eight hours.
20 Chronic occupational exposures to less than 85 dB (or 80 dB, depending on the country) are
21 deemed safe. In *Pjvk*^{-/-} mice, a single exposure to 63 dB $L_{EX,8 \text{ hour}}$ increased hearing
22 thresholds by 30 dB, with full recovery occurring after about two weeks. By contrast, a ten-
23 times more energetic exposure to a $L_{EX,8 \text{ hour}}$ of 73 dB in wild-type mice of the same strain
24 produces only an 18 dB shift in threshold, with a recovery time of 12 hours (Housley et al.,
25 2013). This hypersensitivity of *Pjvk*^{-/-} mice to noise suggests that the $L_{EX,8 \text{ hour}}$ of about 83

1 dB for a cage of 10 pups, is sufficient to account for permanent hearing loss in these *Pjvk*^{-/-}
2 pups, whilst some of those housed in small numbers in quiet rooms can display near-normal
3 hearing thresholds (see Figure 1C). Likewise, the auditory function of DFNB59 patients was
4 transiently affected by a 57 dB L_{EX,8 hour} exposure, routinely used in ABR tests.

5 NIHL involves the excessive production of ROS, overwhelming the anti-oxidant defense
6 system and causing irreversible oxidative damage to DNA, proteins, and lipids within the
7 cell (Henderson et al., 2006). Noise-induced oxidative stress results in the production of
8 H₂O₂ and other ROS as by-products, thought to derive from the intense solicitation of
9 mitochondrial activity. Several mouse mutants with mitochondrial defects are prone to
10 NIHL (Ohlemiller et al., 1999), including mice lacking sirtuin 3, a mitochondrial NAD⁺-
11 dependent deacetylase (Brown et al., 2014). Our studies of pejvakin-deficient mouse
12 mutants and rescue experiments targeting the hair cells and auditory neurons unambiguously
13 show that IHCs, OHCs, primary auditory neurons and neurons of the cochlear nucleus are
14 hypervulnerable to sound in the absence of pejvakin, which is consistent with previous
15 results showing that hair cells and neurons of the auditory system are targets of NIHL
16 (Wang et al., 2002; Kujawa & Liberman, 2009; Imig and Durham, 2005). However, our
17 study goes one step further, by implicating a possible common mechanism: peroxisomal
18 failure, the importance of which is demonstrated by the impairment of the redox
19 homeostasis caused by pejvakin deficiency. It also reveals a major cause of the unusually
20 high level of phenotypic variability observed in pejvakin-deficient mice and humans: the
21 difference in sound-exposure and the inability of the defective peroxisomes to cope with the
22 resulting activity-dependent oxidative stress. Incidentally, this can account for the apparent
23 paradox that mice carrying the R183W mutation in pejvakin displayed a much more severe
24 neural pathway defect than the *Pjvk*^{-/-} mice (Delmaghani et al., 2006). Due to the
25 preservation of hair cell functions, the auditory neurons of R183W mutant mice should be

1 strongly stimulated, whereas the early permanent damage to cochlear hair cells in *Pjvk*^{-/-}
2 mice acts as a protective "muffler" of the neuronal pathway.

3 In mammals, the number and metabolic functions of peroxisomes differ between cell
4 types. However, all cell types are able to adapt rapidly to modifications in physiological
5 conditions by changing the number, shape, size, and molecular content of peroxisomes,
6 resulting in considerable functional plasticity of these organelles (Schrader et al., 2012;
7 Smith and Aitchison, 2013). Our experiments on *Pjvk*^{-/-} and *Pjvk*^{+/+} mouse embryonic
8 fibroblasts stressed with H₂O₂ showed that pejkakin is critically involved in the oxidative
9 stress-induced proliferation of peroxisomes through growth and fission of pre-existing
10 peroxisomes. Although the molecular machinery underlying this adaptive process is still
11 poorly understood, the specific involvement of Pex11 α that recruits COP I has been reported
12 (Li et al., 2002; Passreiter et al., 1998). Of note, the absence of pejkakin only affects the
13 proliferation of peroxisomes from pre-existing peroxisomes, but not the constitutive
14 biogenesis of this organelle. Accordingly, structural abnormalities of peroxisomes in *Pjvk*^{-/-}
15 mice became apparent only after hearing onset, in the context of the oxidative stress
16 produced by noise-exposure. By contrast, the *PEX* gene defects causing Zellweger syndrome
17 spectrum (ZSS) disorders (Waterham & Ebberink, 2012) and rhizomelic chondrodysplasia
18 punctata affect the constitutive biogenesis of peroxisomes. Hearing impairment in ZSS
19 disorders involves a severe impairment of neuronal conduction, and has been attributed to
20 defects in the synthesis of two essential myelin sheath components — plasmalogens and
21 docosahexaenoic acid —, which is critically dependent on peroxisomes. Our results suggest
22 that ZSS also includes a defective redox balance in the hair cells and neurons of the auditory
23 system.

24 In the context of noise-exposure, the upregulation of *Pjvk* transcription in the cochlea
25 and the subsequent peroxisome proliferation in the hair cells and auditory neurons of wild-

1 type mice suggest that pejvakin-dependent peroxisome proliferation in the auditory system
2 is part of the physiological response to high levels of acoustic energy that result in increased
3 amounts of ROS. This and the marked oxidative stress detected in the *Pjvk*^{-/-} cochlea imply
4 that the proliferation of peroxisomes plays an anti-oxidant role, similar to that reported in
5 other cell types (Santos et al., 2005; Diano et al., 2011). The rapid elevation of the hearing
6 threshold in *Pjvk*^{-/-} mice in response to low-energy sounds and the increase in interwave I-IV
7 latency observed in DFNB59 patients within a few seconds are consistent with an activity-
8 dependent H₂O₂ production that, due to impaired cellular redox homeostasis, results in
9 concentrations of H₂O₂ high enough to impact on the activity of various target proteins
10 including ion channels and transporters (Rice, 2011). The worsening of hearing sensitivity,
11 two days later, in the mutant mice lacking pejvakin, exacerbated by putting back the mice in
12 a noisy environment, fits the picture of the absence of sound-induced biogenesis of
13 peroxisomes (with their degeneration occurring in a high acoustic energy environment). We
14 thus conclude that the hypervulnerability of *Pjvk*^{-/-} mice and DFNB59 patients to sound does
15 not result simply from an exacerbation, by sound, of a pre-existing redox balance defect, but
16 is the consequence of the impaired adaptive proliferation of peroxisomes in the absence of
17 pejvakin. Both the defective peroxisome proliferation in IHCs of *Pjvk*^{-/-} mice in response to
18 sound-exposure and its partial recovery by pejvakin cDNA transfer support this conclusion.
19 A full recovery of the adaptive peroxisome proliferation produced by sound-exposure may
20 require higher concentrations of pejvakin or the sound-induced dynamic modulation of *Pjvk*
21 expression (see Figure 6A), which is missing in our rescue experiments (the expression of
22 the pejvakin cDNA being driven by a constitutive promoter).

23 In patients with hearing impairment, the amplification of sound by hearing aids or
24 direct electrical stimulation of the auditory nerve by a cochlear implant delivers a stimulus
25 with an energy level similar to that shown here to worsen the hearing impairment of *Pjvk*^{-/-}

1 mice within one minute of sound exposure. Therefore, in cases of peroxisomal deficiency, as
2 in DFNB59, specific protection against redox homeostasis failure is essential, and patients
3 with such conditions should avoid noisy environments. N-acetyl cysteine was the only
4 antioxidant drug tested here to display some, albeit limited, efficacy. By contrast AAV-
5 mediated gene therapy, could potentially provide full protection. Finally, deciphering the
6 sound stress-induced protective signaling pathway involving pejvakin, and possibly
7 cyclophilin A, c-dopachrome tautomerase, and Mpv17, might lead to the discovery of
8 therapeutic agents for NIHL.

9

10 **EXPERIMENTAL PROCEDURES**

11

12 **Audiological studies in mice**

13 Auditory tests were performed in an anechoic room, on anesthetized animals for which core
14 temperature was maintained at 37°C (see Extended Experimental Procedures).

15

16 **Audiological tests in patients**

17 Informed consent was obtained from all the subjects included in the study. Pure-tone
18 audiometry was performed, with air- and bone-transmitted tones. Hearing impairment was
19 assessed objectively, by measuring ABRs and transient-evoked otoacoustic emissions
20 (TEOAEs). The nonlinear TEOAE recording procedure was used (derived from the ILO88
21 system), making it possible to extract TEOAEs from linear reflection artifacts from the
22 middle ear, and to evaluate background noise. TEOAE responses were analyzed in 1 kHz-
23 wide bands centered on 1, 2, 3 and 4 kHz.

24

25 **Generation of an anti-pejvakin monoclonal antibody**

1 The 3'-end of the coding sequence of the *Pjvk* cDNA (accession number NM_001080711.2)
2 was inserted into a pGST-parallel-2 vector (derived from pGEX-4T-1; Amersham). The
3 resulting construct, encoding the C-terminal region of pejvakin (residues 290-352; accession
4 number NP_001074180.1) fused to an N-terminal glutathione *S*-transferase tag, was
5 introduced into *E. coli* BL21-Gold (DE3) competent cells (Stratagene). The pejvakin protein
6 fragment was purified on a glutathione-Sepharose 4B column, then subjected to size-
7 exclusion chromatography and used as the antigen for immunization. Antibodies were
8 produced by immunizing *Pjvk*^{-/-} mice. An IgG monoclonal antibody (K_D of 6 × 10⁻⁸ M),
9 Pjvk-G21, was selected by ELISA on immunogen-coated plates.

10

11 **Determination of total and oxidized glutathione**

12 Total glutathione (GSH + GSSG) and oxidized glutathione (GSSG) levels were determined
13 as described by Rahman et al. (2006). Total glutathione and GSSG levels were evaluated by
14 spectrometry at 405 nm. GSH concentration was calculated by subtracting the concentration
15 of GSSG from the total glutathione concentration. Three independent experiments were
16 performed, in P21 *Pjvk*^{+/+} and *Pjvk*^{-/-} mice.

17

18 **Statistical analyses**

19 Statistical analyses were performed using GraphPad. Data were analyzed by either paired or
20 unpaired Student's t-tests, and, for more than two groups, we used one-way or two-way
21 ANOVA analyses of variance. Statistical significance is defined as $p < 0.05$ and indicated
22 by asterisks.

23

24 **SUPPLEMENTAL INFORMATION**

1 The supplemental information includes Extended Experimental Procedures, seven figures,
2 and one table.

3

4 **AUTHOR CONTRIBUTIONS**

5 C.P. and P.A. designed study. P.A. and S.D. analyzed auditory tests in patients. P.A., S.D.,
6 and F.G. performed audiological tests in mice. S.D. performed recombination experiments
7 on embryonic stem cells to produce knockout mice, and transcriptomic and biochemical
8 studies. A.A. produced recombinant proteins. S.Da. produced the monoclonal antibody. I.P.,
9 J.D., and S.D. performed cell transfections, immunohistolabeling experiments. I.P. and S.D.
10 produced mouse embryonic fibroblasts. N.T., M.T., M.L., S.D., and S.S. performed
11 ultrastructural studies. S.D., A.M., and A.E. supervised by S.S., performed rescue
12 experiments in mice. M.B. and D.D. performed electrophysiological experiments in mice.
13 T.Z., M.A., and E.S.V. performed mitochondrial physiological analysis. C.P., P.A., S.D.,
14 J.D., and J.-P.H. wrote the manuscript.

15

16 **ACKNOWLEDGMENTS**

17 We thank M. Aghaie for assistance with the collection of clinical data, M. Mobasheri for
18 audiological tests in the patients, F. Langa-Vives and the *Centre d'ingénierie génétique*
19 *murine* platform for producing *Pjvk*^{-/-} recombinant mice, the *Transcriptome et épigénome*
20 platform for microarray experiments, P. Aubourg for fruitful discussions, and M. Ricchetti
21 and J. Boutet de Monvel for critical reading of the manuscript. This study was supported by
22 grants from Louis-Jeantet Foundation, ANR – NKTH “HearDeafTreat” 2010-INTB-1402-
23 01, European Research Council (ERC)-Hair Bundle (ERC-2011-ADG-294570), Humanis
24 Novalis-Taitbout, Réunica-Prévoyance, BNP Paribas, and French state program
25 “Investissements d’Avenir” (ANR-10-LABX-65) to C.P.

26

27 **REFERENCES**

28 Ashmore, J. (2008). Cochlear outer hair cell motility. *Physiol. Rev.* 88, 173-210.
29 Avan, P., Buki, B., and Petit, C. (2013). Auditory distortions: origins and functions.
30 *Physiological reviews* 93, 1563-1619.

1 Borck, G., Rainshtein, L., Hellman-Aharony, S., Volk, A.E., Friedrich, K., Taub, E., Magal,
2 N., Kanaan, M., Kubisch, C., Shohat, M., *et al.* (2012). High frequency of autosomal-
3 recessive DFNB59 hearing loss in an isolated Arab population in Israel. *Clin. Genet.* 82,
4 271-276.

5 Brown, K.D., Maqsood, S., Huang, J.Y., Pan, Y., Harkcom, W., Li, W., Sauve, A., Verdin,
6 E., and Jaffrey, S.R. (2014). Activation of SIRT3 by the NAD(+) precursor nicotinamide
7 riboside protects from noise-induced hearing loss. *Cell Metab.* 20, 1059-1068.

8 Cody, A.R., and Johnstone, B.M. (1981). Acoustic trauma: single neuron basis for the "half-
9 octave shift". *J. Acoust. Soc. Am.* 70, 707-711.

10 Collin, R.W., Kalay, E., Oostrik, J., Caylan, R., Wollnik, B., Arslan, S., den Hollander, A.I.,
11 Birinci, Y., Lichtner, P., Strom, T.M., *et al.* (2007). Involvement of DFNB59 mutations in
12 autosomal recessive nonsyndromic hearing impairment. *Hum. Mutat.* 28, 718-723.

13 Delmaghani, S., del Castillo, F.J., Michel, V., Leibovici, M., Aghaie, A., Ron, U., Van Laer,
14 L., Ben-Tal, N., Van Camp, G., Weil, D., *et al.* (2006). Mutations in the gene encoding
15 pejvakin, a newly identified protein of the afferent auditory pathway, cause DFNB59
16 auditory neuropathy. *Nat. Genet.* 38, 770-778.

17 Diano, S., Liu, Z.W., Jeong, J.K., Dietrich, M.O., Ruan, H.B., Kim, E., Suyama, S., Kelly,
18 K., Gyengesi, E., Arbiser, J.L., *et al.* (2011). Peroxisome proliferation-associated control of
19 reactive oxygen species sets melanocortin tone and feeding in diet-induced obesity. *Nat.*
20 *Med.* 17, 1121-1127.

21 Ebberink, M.S., Koster, J., Visser, G., Spronsen, F., Stolte-Dijkstra, I., Smit, G.P., Fock,
22 J.M., Kemp, S., Wanders, R.J., and Waterham, H.R. (2012). A novel defect of peroxisome
23 division due to a homozygous non-sense mutation in the PEX11beta gene. *J. Med. Genet.*
24 49, 307-313.

25 Ebermann, I., Walger, M., Scholl, H.P., Charbel Issa, P., Luke, C., Nurnberg, G., Lang-
26 Roth, R., Becker, C., Nurnberg, P., and Bolz, H.J. (2007). Truncating mutation of the
27 DFNB59 gene causes cochlear hearing impairment and central vestibular dysfunction. *Hum.*
28 *Mutat.* 28, 571-577.

29 Henderson, D., Bielefeld, E.C., Harris, K.C., and Hu, B.H. (2006). The role of oxidative
30 stress in noise-induced hearing loss. *Ear Hearing* 27, 1-19.

31 Housley, G.D., Morton-Jones, R., Vlajkovic, S.M., Telang, R.S., Paramanathasivam, V.,
32 Tadros, S.F., Wong, A.C., Froud, K.E., Cederholm, J.M., Sivakumaran, Y., *et al.* (2013).
33 ATP-gated ion channels mediate adaptation to elevated sound levels. *Proc. Natl. Acad. Sci.*
34 *U.S.A.* 110, 7494-7499.

1 Imig, T.J., and Durham, D. (2005). Effect of unilateral noise exposure on the tonotopic
2 distribution of spontaneous activity in the cochlear nucleus and inferior colliculus in the
3 cortically intact and decorticate rat. *J. Comp. Neurol.* *490*, 391-413.

4 Kujawa, S.G., and Liberman, M.C. (2009). Adding insult to injury: cochlear nerve
5 degeneration after "temporary" noise-induced hearing loss. *J. Neurosci.* *29*, 14077-14085.

6 Li, X., Baumgart, E., Dong, G.X., Morrell, J.C., Jimenez-Sanchez, G., Valle, D., Smith, K.D.
7 and Gould, S.J. (2002). PEX11alpha is required for peroxisome proliferation in
8 response to 4-phenylbutyrate but is dispensable for peroxisome proliferator-activated
9 receptor alpha-mediated peroxisome proliferation. *Mol. Cell. Biol.* *22*, 8226-8240.

10 Lopez-Huertas, E., Charlton, W.L., Johnson, B., Graham, I.A., and Baker, A. (2000). Stress
11 induces peroxisome biogenesis genes. *EMBO J.* *19*, 6770-6777.

12 Mizuno, Y., Kurochkin, I.V., Herberth, M., Okazaki, Y., and Schonbach, C. (2008).
13 Predicted mouse peroxisome-targeted proteins and their actual subcellular locations. *BMC*
14 *Bioinform.* *9 Suppl 12*, S16.

15 Møller, A.R., Jannetta, P.J. (1983). Interpretation of brainstem auditory evoked potentials:
16 results from intracranial recordings in humans, *Scand Audiol.* *12*, 125-33.

17 Ohlemiller, K.K., Wright, J.S., and Dugan, L.L. (1999). Early elevation of cochlear reactive
18 oxygen species following noise exposure. *Audiol. Neurootol.* *4*, 229-236.

19 Oliver, D., Taberner, A.M., Thurm, H., Sausbier, M., Arntz, C., Ruth, P., Fakler, B., and
20 Liberman, M.C. (2006). The role of BKCa channels in electrical signal encoding in the
21 mammalian auditory periphery. *J. Neurosci.* *26*, 6181-6189.

22 Passreiter, M., Anton, M., Lay, D., Frank, R., Harter, C., Wieland, F.T., Gorgas, K., and
23 Just, W.W. (1998). Peroxisome biogenesis: involvement of ARF and coatomer. *J. Cell Biol.*
24 *141*, 373-383.

25 Rahman, I., Kode, A., and Biswas, S.K. (2006). Assay for quantitative determination of
26 glutathione and glutathione disulfide levels using enzymatic recycling method. *Nat. Protoc.*
27 *1*, 3159-3165.

28 Rice, M.E. (2011). H₂O₂: a dynamic neuromodulator. *Neuroscientist* *17*, 389-406.

29 Robles, L., and Ruggero, M.A. (2001). Mechanics of the mammalian cochlea. *Physiol. Rev.*
30 *81*, 1305-1352.

31 Santos, M.J., Quintanilla, R.A., Toro, A., Grandy, R., Dinamarca, M.C., Godoy, J.A., and
32 Inestrosa, N.C. (2005). Peroxisomal proliferation protects from beta-amyloid
33 neurodegeneration. *J. Biol. Chem.* *280*, 41057-41068.

1 Schrader, M., Bonekamp, N.A. and Islinger, M. (2012) Fission and proliferation of
2 peroxisomes. *Biochim. Biophys. Acta* 1822, 1343-1357.
3 Schrader, M., and Fahimi, H.D. (2006). Peroxisomes and oxidative stress. *Biochim.*
4 *Biophys. Acta* 1763, 1755-1766.
5 Schwander, M., Sczaniecka, A., Grillet, N., Bailey, J.S., Avenarius, M., Najmabadi, H.,
6 Steffy, B.M., Federe, G.C., Lagler, E.A., Banan, R., *et al.* (2007) A forward genetics screen
7 in mice identifies recessive deafness traits and reveals that pejvakin is essential for outer hair
8 cell function. *J. Neurosci.* 27, 2163-2175.
9 Smith, J.J., and Aitchison, J.D. (2013). Peroxisomes take shape. *Nat. Rev. Mol. Cell Biol.*
10 14, 803-817.
11 Starr, A. & Rance, G. (2015). Auditory neuropathy. *Handb Clin Neurol.* 129, 495-508.
12 Tang, X.D., Garcia, M.L., Heinemann, S.H., and Hoshi, T. (2004). Reactive oxygen species
13 impair Slo1 BK channel function by altering cysteine-mediated calcium sensing. *Nat. Struct.*
14 *Mol. Biol.* 11, 171-178.
15 Wang, Y., Hirose, K., and Liberman, M.C. (2002). Dynamics of noise-induced cellular
16 injury and repair in the mouse cochlea. *J. Assoc. Res. Otolaryngol.* 3, 248-268.
17 Waterham, H.R., and Ebberink, M.S. (2012). Genetics and molecular basis of human
18 peroxisome biogenesis disorders. *Biochim. Biophys. Acta* 1822, 1430-1441.

19
20

21

22 **FIGURE LEGENDS**

23 **Figure 1. Hearing loss variability and greater sensitivity to controlled sound-exposure**
24 **in *Pjvk*^{-/-} mice.** (A) ABR thresholds at 10 kHz in P30 *Pjvk*^{+/+} (n = 26 mice) and *Pjvk*^{-/-} (n =
25 48 mice) littermates. (B) DPOAE thresholds at 10 kHz in P30 *Pjvk*^{+/+} (n = 14 mice) and
26 *Pjvk*^{-/-} (n = 48 mice) littermates. In ears with no DPOAE, even at 75 dB SPL (the highest
27 sound intensity tested), DPOAE thresholds were arbitrarily set at 80 dB SPL. (C)
28 Relationship between the number of pups raised together (determining sound levels in the
29 immediate environment) and ABR thresholds at 10 kHz in P21 *Pjvk*^{-/-} pups. Inset: Time-
30 frequency analysis of a mouse pup's vocalization. Pup calls from P0 to P21 form harmonic
31 series of about 5 kHz, with the most energetic harmonic at about 10 kHz. In a 12-pup litter,

1 call levels reach 105 ± 5 dB SPL at the entrance to the ear canals of the pups. (D) ABR
2 thresholds at 10 kHz in P30 $Pjvk^{+/+}$ and $Pjvk^{-/-}$ mice before (dots) and after (crosses)
3 controlled sound-exposure. n.s., not significant; *** $p < 0.001$.

4

5 **Figure 2. Effects on auditory function of brief exposure to moderately intense stimuli**
6 **in $Pjvk^{+/+}$, $Pjvk^{-/-}$, and $Pjvk^{fl/fl}Myo15-cre^{+/-}$ mice.** (A-C) ABR wave I amplitude (A),
7 DPOAE amplitude (B) and ABR interwave I-IV latency (C) in $Pjvk^{+/+}$, $Pjvk^{-/-}$ and
8 $Pjvk^{fl/fl}Myo15-cre^{+/-}$ mice, before (dots) and after (crosses) controlled sound-exposure,
9 revealing the hypervulnerability to sound of both types of cochlear hair cells (IHCs and
10 OHCs) and the auditory pathway, only in $Pjvk^{-/-}$ mice. (D) EEBR wave E IV amplitude
11 before and after controlled electrical exposure in $Pjvk^{-/-}$ and $Pjvk^{fl/fl}Myo15-cre^{+/-}$ mice,
12 abnormal and hypervulnerable only when pejvakin is absent from auditory neurons ($Pjvk^{-/-}$
13 mice). (E and F) Examples of ABRs in $Pjvk^{-/-}$ and $Pjvk^{fl/fl}Myo15-cre^{+/-}$ mice: the latency of
14 wave I is affected by controlled sound-exposure in both mutant mice, and wave IV displays
15 an additional increase in latency only in $Pjvk^{-/-}$ mice. (G-I) Examples of EEBRs in $Pjvk^{+/+}$
16 (G), $Pjvk^{-/-}$ (H), and $Pjvk^{fl/fl}Myo15-cre^{+/-}$ (I) mice; EEBRs are affected by controlled
17 electrical exposure only in $Pjvk^{-/-}$ mice. (J-L) Neuronal function rescue in $Pjvk^{-/-}$ mice by
18 transduction with AAV8-Pjvk: effects on ABR interwave I-IV latency (J), on EEBR wave E
19 IV amplitude and its hypervulnerability (K), and on EEBR interwave E II-E IV latency (one
20 example is shown in L, to be compared with H). Vertical arrows indicate the positions of
21 waves I and IV on ABR traces, and of waves E II and E IV on EEBR traces. n.s., not
22 significant; *** $p < 0.001$. Error bars represent the SD. See also Figure S2A.

23

24 **Figure 3. Hypervulnerability to sound in DFNB59 patients.** (A) ABR waves I, III, and V
25 (vertical arrows) in one ear of a patient carrying the *PJVK* p.T54I mutation, in response to

1 250, 500, and 1000 impulse stimuli (clicks) at 99 dB nHL. (B) Repeated ABRs after 10
2 minutes of silence, with an even larger vulnerability of waves I, III, and V. (C and D)
3 Distributions of the amplitude (C) and latency (D) of ABR wave V in the tested sample of
4 p.T54I patients (n = 8 ears), and in a control group of patients (n = 13) with cochlear hearing
5 impairment and matched ABR thresholds, before and after exposure to clicks #250 to #1000.
6 Boxes extend from the 25th to the 75th percentile. Horizontal bars and vertical bars indicate
7 median values and extremes, respectively. Unlike the unaffected controls, all p.T54I patients
8 displayed markedly decreased amplitudes and increased latencies.

9

10 **Figure 4. Oxidative stress and ROS-induced cell damage in the *Pjvk*^{-/-} cochlea.** (A)
11 Lower reduced-glutathione (GSH) (left bar chart) and higher oxidized-glutathione (GSSG)
12 (middle bar chart) contents, and lower GSH:GSSG ratio, in P21 *Pjvk*^{-/-} than *Pjvk*^{+/+} mice
13 (right bar chart). Error bars represent the SEM of 3 independent experiments. See also
14 Figure S3. (B) Marked decrease in the BK α -subunit expression in *Pjvk*^{-/-} IHCs. Left: P20
15 *Pjvk*^{+/+} and *Pjvk*^{-/-} IHCs, immunolabeled for the BK α -subunit. Scale bars are 5 μ m. Right:
16 quantitative analysis of BK channel clusters. Error bars represent the SD. See also Figure
17 S7B. * p < 0.05, *** p < 0.001.

18

19 **Figure 5. Pejvakin is a peroxisome-associated protein involved in the oxidative stress-**
20 **induced peroxisomal proliferation.** (A, B) Immunolabeling of peroxisome membrane
21 protein 70 (PMP70) and endogenous pejvakin in a HepG2 cell (A) and two P20 *Pjvk*^{+/+} and
22 *Pjvk*^{-/-} IHCs (B) showing their colocalization. See also Figure S5B. (C) Number of
23 peroxisomes per *Pjvk*^{+/+} and *Pjvk*^{-/-} MEFs subjected to 0.5 mM H₂O₂ compared to untreated
24 (n = 30 cells for each condition). The number of peroxisomes increased only in *Pjvk*^{+/+} cells.
25 See also Figure S6A. (D) Untransfected HeLa cells (NT), and transfected cells producing
26 EGFP alone or with either the wild-type pejvakin (Pjvk) or various mutated forms (different

1 missense mutations, p.T54I, p.R183W, p.C343S, and p.V330Lfs*7, reported in DFNB59
2 patients). Right panel: Bar chart showing the numbers of peroxisome per cell 48 hours after
3 transfection. There were 33% more peroxisomes in cells producing Pjvk (n = 200) than in
4 cells producing EGFP alone (n = 150). Left panel: For every range of enlarged peroxisome
5 size, x (0.6-0.8 μm , 0.8-1.0 μm , and $> 1.0 \mu\text{m}$), in two perpendicular directions, the
6 proportion of cells containing at least one peroxisome in that range is higher for cells
7 producing any mutated form of pejvakin (n = 80) than for cells producing Pjvk (n = 320).
8 See also Figure S6B. (E) Abnormalities in shape and distribution of peroxisomes in mature
9 *Pjvk*^{-/-} OHCs detected by transmission electron microscopy. P30 *Pjvk*^{+/+} (left panel) and
10 *Pjvk*^{-/-} (middle and right panels) OHCs. Insets (middle panel) show enlarged views of
11 individual peroxisomes: peroxisomes are grouped just under the cuticular plate (CP)
12 (arrowheads), with none detected in the perinuclear region (n = 33 sections, upper bar chart).
13 In *Pjvk*^{-/-} OHCs, some peroxisomes remain under the cuticular plate (arrowheads), but
14 catalase-containing structures, misshapen peroxisomes (arrows), are detected in the
15 perinuclear region (n = 24 sections, upper bar chart). Peroxisomes located under the
16 cuticular plate are larger in *Pjvk*^{-/-} (n = 92 peroxisomes) than in *Pjvk*^{+/+} (n = 89 peroxisomes)
17 OHCs (lower bar chart). N: cell nucleus. ** p < 0.01, *** p < 0.001. Error bars represent the
18 SEM. Scale bars are 2 μm in (A) and (B), and 0.5 μm in (E).

19

20 **Figure 6. Effect of exposure to loud sounds on the cochlear expression of *Pjvk* and the**
21 **number of peroxisomes in cochlear hair cells and ganglion neurons. (A) *Pjvk* and *c-Dct*,**
22 ***CypA*, *Mpv17*, *Gpx2* transcript levels (genes downregulated in *Pjvk*^{-/-} mice) assessed by**
23 **quantitative RT-PCR in the organ of Corti of P21 *Pjvk*^{+/+} mice, 1, 3, 6, and 18 hours after**
24 **sound-exposure (5-20 kHz, 105 dB SPL for 1 hour). *Pjvk* transcript levels increased by a**
25 **factor of 2 to almost 4 from 1 to 6 hours, and returned to pre-exposure levels at 18 hours.**

1 The levels of *c-Dct*, *CypA*, and *Mpv17* but not *Gpx2* transcripts followed similar time
2 courses. The levels of *c-Fos* and *Hsp70* transcripts were used as positive controls. See also
3 Figure S4B. (B) Peroxisome proliferation in the hair cells and cochlear ganglion neurons of
4 P21 *Pjvk*^{+/+} mice after sound-exposure (same conditions as in A). Peroxisomes counted 48
5 hours after exposure, in OHCs and IHCs (whole-mount preparations), and in the dendrites of
6 ganglion neurons (cryosections). OHCs, IHCs, and neuronal processes, stained for F-actin,
7 myosin VI, and neurofilament protein NF200, respectively, allow to identify peroxisomes
8 located inside hair cells or neurons. For OHCs, both a lateral view and a transverse optical
9 section at the level of the cuticular plate (see scheme on the right) are shown. The number of
10 peroxisomes increased in OHCs, IHCs, and dendrites after sound-exposure. The
11 peroxisomes are located below the cuticular plate (CP) and throughout the cytoplasm in
12 OHCs and IHCs, respectively. N: cell nucleus. *** p < 0.001. Error bars represent the SEM.
13 Scale bars are 5 μm.

14

15 **Figure 7. Therapeutic approaches in *Pjvk*^{-/-} mice.** (A-C) Effect of N-acetyl cysteine on
16 auditory function in *Pjvk*^{-/-} mice. (A) ABR thresholds in untreated and N-acetyl cysteine
17 (NAC)-treated P21 *Pjvk*^{-/-} mice, showing a moderate improvement in treated mice. (B) ABR
18 wave I amplitude (which relates to the number of synchronously responding primary
19 auditory neurons) for 10 kHz tone bursts in *Pjvk*^{+/+}, untreated *Pjvk*^{-/-}, and NAC-treated *Pjvk*^{-/-}
20 mice at P21, showing normalization in treated mice. (C) EEER wave E IV amplitude before
21 (dots) and after (crosses) controlled electrical stimulation of the cochlear nerve at 200
22 impulses/s for 1 minute in *Pjvk*^{+/+}, untreated *Pjvk*^{-/-}, and NAC-treated *Pjvk*^{-/-} mice, showing
23 that the hypersensitivity of the auditory pathway in *Pjvk*^{-/-} mice responds to NAC treatment.
24 (D-I) AAV2/8-mediated transfer of the pejkakin cDNA in the cochlea of *Pjvk*^{-/-} mice. See
25 also Figure S2B. (D) Beneficial effect of viral transduction on ABR thresholds at 10, 15, and

1 20 kHz in treated (AAV2/8-Pjvk) vs. untreated *Pjvk*^{-/-} mice. (E) Improved ABR wave I
2 latency in treated vs. contralateral, untreated ears. (F, H) Improved DPOAE threshold (F)
3 and ABR wave I amplitude (H) at 10 kHz in treated vs. contralateral, untreated ears. (G)
4 Correlation between DPOAE thresholds and the proportion of EGFP-tagged (i.e.
5 transduced) outer hair cells (OHCs). Note that the six untreated ears displayed no recordable
6 DPOAE (threshold arbitrarily set at 80 dB SPL, red diamond). (I) Correlation between ABR
7 wave I amplitude at 10 kHz, 105 dB SPL and the proportion of EGFP-tagged (i.e.
8 transduced) IHCs. Error bars represent the SD. (J) Beneficial effect of pejvakin cDNA
9 transfer on impaired sound-induced proliferation of peroxisomes in IHCs of *Pjvk*^{-/-} mice.
10 Upper and lower panels illustrate and quantify (bar charts) the decreased number of
11 peroxisomes (with some peroxisomes displaying structural abnormalities, arrowhead) in
12 untreated mice 48 hours after sound-exposure (5-40 kHz, 105 dB SPL for 1 hour) and the
13 partial recovery of the adaptive peroxisome proliferation in treated mice, respectively. Error
14 bars represent the SEM. n.s., not significant; * $p < 0.05$, ** $p < 0.01$, *** $p < 0.001$.

1 **Supplemental Information**

2 **EXTENDED EXPERIMENTAL PROCEDURES**

3 **Animal handling**

4 Animals were housed in the Institut Pasteur animal facilities, which are accredited by the
5 French Ministry of Agriculture for experimentation on live mice (accreditation 75-15-01,
6 issued on September 6th, 2013 in application of the French and European regulations on the
7 care and protection of laboratory animals (EC Directive 2010/63, French Law 2013-118,
8 February 6th, 2013). The corresponding author confirms that the protocols were approved by
9 the veterinary staff of the Institut Pasteur animal facility, and were performed in accordance
10 with the NIH Animal Welfare Insurance #A5476-01 issued on July 31st, 2012.

11

12 **Gene targeting, genotyping, and RT-PCR**

13 We designed a targeting vector, in which exon 2 of *Pjvk* and the neomycin selection cassette
14 (*PGK-neo*) were flanked by loxP sites. A negative selection cassette encoding the diphtheria
15 toxin A fragment was inserted at the 3'-end of the *Pjvk* targeting sequence (Figure S1A).
16 CK35 embryonic stem (ES) cells (Kress et al., 1998), derived from a 129/Sv mouse embryo,
17 were electroporated with the purified, linearized targeting vector, and plated on G418
18 selective medium, as previously described (Matise et al., 1999). Approximately 300
19 recombinant ES cell clones were obtained, 12 of which were correctly targeted. The
20 homologous recombinant event was confirmed by PCR, with primers specific for the 5' and
21 3' genomic sequences outside the region used in the targeting vector, and specific for the
22 *PGK-neo* sequence. The sequences of the PCR primers used to genotype the floxed *Pjvk*
23 allele are available on request. The integration of the recombinant DNA construct was
24 confirmed by Southern blot analysis and PCR amplification of genomic DNA extracted
25 from mouse tails. Two independent clones were used to create chimeric mice displaying

1 germline transmission, by injection into C57BL/6J blastocysts. Male chimeras were crossed
2 with C57BL/6J females to produce heterozygous animals. Mice heterozygous for the floxed
3 *Pjvk* allele were crossed with PGK-cre^m deleter mice carrying the cre recombinase gene
4 driven by the early-acting ubiquitous phosphoglycerate kinase-1 gene promoter (Lallemand
5 et al., 1998), to obtain *Pjvk*-knockout (*Pjvk*^{-/-}) mice. The targeted deletion of exon 2 was
6 confirmed by PCR analysis.

7 Mice with a conditional knockout of *Pjvk* (*Pjvk*^{fl/fl}*Myo15*-cre^{+/-}), in which expression of the
8 deleted *Pjvk* was restricted to the inner ear sensory cells, were generated by crossing mice
9 carrying the floxed *Pjvk* allele with transgenic mice expressing the Cre recombinase gene
10 under the control of the myosin-15 gene promoter (Caberlotto et al., 2011). Auditory
11 function was analyzed in ubiquitous knockout and conditional knockout mice. All studies
12 were performed in a C57BL/6J-129/Sv mixed genetic background.

13 For RT-PCR analysis of *Pjvk* transcript levels, total RNA was extracted from the inner ears
14 of *Pjvk*^{+/+} and *Pjvk*^{-/-} P7 mice with the NucleoSpin[®] RNA II kit (Macherey-Nagel). The
15 sequences of the PCR primers used to characterize the *Pjvk* transcript (Figure S1B) are
16 available on request.

17

18 **Auditory tests, controlled sound-exposure, and controlled electrical stimulation of the** 19 **auditory nerve in mice**

20 Mice were anesthetized by intraperitoneal injection of a mixture of ketamine and
21 levomepromazin (100 mg/kg; 5 mg/kg), and their core temperature was maintained at 37°C
22 with the aid of a servo-controlled heating pad. The DPOAE at a frequency $2f_1-f_2$ was
23 recorded in response to two primary tones of similar energy levels, f_1 and f_2 , with $f_2/f_1 = 1.20$
24 (Cub[®]Dis system, Mimoso Acoustics; ER10B microphone, Etymotic Res.). Frequency f_2 was
25 swept at 1/10th octave steps from 4 to 20 kHz, and DPOAE threshold was plotted against

1 frequency f_2 (primary tone levels increased from 20 to 70 dB SPL in 10 dB steps, then to 75
2 dB SPL). The DPOAE threshold was defined as the smallest primary level eliciting a
3 detectable DPOAE. The ABRs in response to calibrated short tone bursts in the 5-40 kHz
4 range (repetition rate 17/s) were derived by the synchronous averaging of
5 electroencephalograms recorded between subcutaneous stainless steel electrodes at the
6 vertex and ipsilateral mastoid, with the help of a standard digital averaging system
7 (CED1401+). A hundred responses to the tone bursts were averaged, except within 10 dB of
8 the ABR threshold (defined as the smallest tone-burst level giving rise to at least one
9 repeatable wave above background noise levels, 150 nV in an anesthetized animal), for
10 which 300 tone bursts were used. Once ABR thresholds had been assessed, ABRs in
11 response to 95 and 105 dB SPL tone bursts (100 averages) were collected for the analysis of
12 suprathreshold ABR waveforms, amplitudes and latencies. Controlled sound-exposure was
13 applied with the same acoustic probe used for ABRs, without moving the sound delivery
14 system, so that pre- and post-exposure ABRs shared the same calibration. The intense
15 stimuli were the same tone bursts used for ABR measurements at 105 dB SPL, presented
16 1000 times, at the same repetition rate of 17/s.

17 The eighth cranial nerve was stimulated electrically with a silver electrode placed in the
18 round-window niche and excited by biphasic electrical impulses (neutral electrode in neck
19 muscles; peak amplitude of electrical stimulus about 0.5 V; duration of the positive and
20 negative phases 150 μ s; adjustable repetition rate). EEERs were extracted with the same
21 setup as for ABRs (Roux et al., 2006), in response to 100 electrical impulses presented with
22 alternating polarities (repetition rate 17/s). The EEER threshold was defined as the smallest
23 electrical amplitude eliciting repeatable waves above the level of background noise (the
24 same as for ABRs), labeled from E II to E IV in reference to their ABR equivalents, II-IV
25 (Henry, 1979). Controlled electrical stimulation was applied at 5 dB above the EEER

1 detection threshold, with a 200 Hz repetition rate. The silver electrode on the round window
2 was occasionally also used to record compound action potentials (CAPs) in response to the
3 same tone bursts used for ABR studies (means of 32 presentations, repetition rate 17/s),
4 before EEBR data collection. These recordings were used to check that CAP thresholds and
5 ABR thresholds were within 2 dB of each other at all frequencies, and the exact position of
6 ABR wave I could be ascertained from the larger wave N1, its equivalent on CAP
7 recordings. This was particularly important in mice with an abnormally small wave I, to
8 prevent incorrect identifications (when wave I was reduced to a very small flattened
9 deflection resembling a summing potential, the slightly larger wave II might have been
10 erroneously labeled wave I on ABR recordings, whereas wave N1, even when small,
11 retained its characteristic shape).

12 The round-window electrode also provided access to the cochlear microphonic potential
13 (CM), with the same setting used for CAP measurements, except that the stimulus polarity
14 was fixed for CM recordings, instead of alternating between rarefaction and condensation
15 tone-bursts for CAP detection. CM is a far-field potential resulting from mechano-electrical
16 transduction currents through the OHCs at the basal end of the cochlea, near the collecting
17 electrode, and is an oscillating change in electric potential at the stimulus frequency.
18 Although its shape is closely similar to that of the stimulus that activates the sound-
19 delivering earphone, it was easily separated from a possible electric artefact radiated by the
20 earphone by its delay of about 0.5 ms after stimulus onset, in relation to sound propagation
21 along the tubing system that connected the earphone to the ear canal of the mouse. Its peak-
22 to-peak amplitude was measured for a stimulus of 5 kHz (a frequency much lower than the
23 best frequency of the responding OHCs, so that CM was independent of their electromotility
24 status) presented at 95 dB SPL.

25

1 **Controlled sound-exposure in DFNB59 patients**

2 We assessed the hypervulnerability to sound of patients, using the minimal sound-exposure
3 eliciting ABRs. ABRs were first recorded in response to 250 impulse stimuli (clicks, with a
4 repetition rate of 20/s) at 99 dB above the normal detection threshold (the maximum level
5 with this equipment, a Vivosonic IntegrityTM Version 4.50), 20-30 dB above the ABR
6 threshold in the tested ear. The averaging was then extended to 500 and 1000 clicks, and
7 wave identification, amplitudes and latencies post click onset were compared for the three
8 averaged ABRs. In control patients, averaging was prolonged until about 4000 responses to
9 clicks had been collected. After a 10-minute pause with no sound stimulus, the procedure
10 was repeated. TEOAEs were averaged just before the first ABR procedure, then just after, in
11 response to 260 series of clicks presented at 40 dB above the normal detection threshold
12 (these clicks were therefore inaudible in patients).

13

14 **Recording of mouse vocalizations**

15 The protocol was adapted from that described by Menuet et al. (2011). The mice were
16 placed in a polyethylene cage covered with a metal wire lid. A free field microphone (type
17 4192, ½-inch, Brüel & Kjaer) was placed 2 cm above the metal lid, in the center of the cage.
18 The microphone output was preamplified (microphone power supply type 2801, Brüel &
19 Kjaer) and digitized by a computer sound card (Dell D830; Dell Inc.) at a sampling rate of
20 192 kHz. Acoustic vocalizations in the 5-90 kHz frequency range were stored online with
21 Adobe Audition 1.5 software. They were analyzed with software developed in Matlab (The
22 MathWorks Inc., MA) providing a spectrographic display of vocalizations in the time-
23 frequency domain, from which the total vocalization time, mean intensity of vocalizations,
24 and spectral complexity of vocalizations were determined.

25

1 **Housing of mice in an acoustically quiet environment**

2 As most of the noise to which young mice are exposed is due to vocalizations (Ehret &
3 Riecke, 2002), we split pups from the same litter into three groups, which were then placed
4 in isolated boxes. The pups were separated before P10, corresponding to several days before
5 hearing onset in mice. The boxes were kept in quiet booths, shielded from the sounds
6 emanating from other cages. The cages of the first group contained two mice and a foster
7 mother, those of the second group contained four mice and a foster mother, and those of the
8 third group contained the remaining pups (6 to 10) and their mother.

9

10 **Quantification of lipid peroxidation**

11 We determined the concentration of malondialdehyde, a by-product of lipid peroxidation,
12 with the thiobarbituric acid-reactive substances assay kit (Cayman Chemical Company) and
13 fluorometry at 590 nm. Three independent experiments were performed. For each assay,
14 cochlear sensory epithelia were microdissected from 30 *Pjvk*^{+/+} and 30 *Pjvk*^{-/-} mice.

15

16 **Plasmids and DNA transfection**

17 The full-length pejavakin cDNA was obtained by RT-PCR on a double-stranded cDNA
18 library prepared from the organs of Corti of P7 C57BL/6 mice. It was inserted into the
19 pIRES2-EGFP vector (Clontech). The mutant pejavakin clones (missense and frameshift
20 mutations) were prepared from the wild-type pejavakin clone with the QuikChange™ Site-
21 Directed Mutagenesis kit (Stratagene). HeLa cells were transiently transfected using
22 Lipofectamine™ 2000 (Invitrogen), according to the manufacturer's instructions.

23

24 **Treatment of mouse embryonic fibroblasts with H₂O₂**

1 Fibroblasts were isolated from mouse embryos at embryonic day 13.5 and cultured as
2 described by Xu (2005). The cells were incubated in DMEM (Gibco) supplemented with 0.1
3 mM β -mercaptoethanol, and 0.5 mM H_2O_2 for 4 hours at 37 °C, under normoxic conditions
4 (95% air). The culture medium was then replaced with H_2O_2 -free medium. Cell viability was
5 checked 18 hours after H_2O_2 treatment, by measuring mitochondrial reductase activity with
6 the MTT (3-(4,5-dimethylthiazol-2-yl)-2,5-diphenyl tetrazolium bromide) (Sigma M2128)
7 assay. A polyclonal antibody against peroxisome membrane protein 70 (PMP70, Abcam
8 ab3421) was used to label peroxisomes.

9

10 **AAV-*Pjvk* viral constructs and intracochlear viral transduction**

11 AAV2/8-*Pjvk*-IRES-EGFP was obtained by inserting the murine pejkakin cDNA flanked by
12 an IRES-EGFP reporter cDNA sequence into the multiple cloning site of the
13 pENN.AAV.CB7.CI.RBG vector (PennVector P1044, Penn Medicine Vector Core -
14 University of Pennsylvania School of Medicine). The virus was produced and titrated by
15 Penn Medicine Vector Core. AAV8-*Pjvk* was produced by inserting the murine pejkakin
16 cDNA into a single-promoter Ad.MAX™ shuttle vector (ITR-CAG-Dfnb59-WPRE-PolyA-
17 ITR; SignaGen Laboratories). The virus was packaged and titrated by SignaGen
18 Laboratories.

19 Intracochlear viral transduction was carried out as described by Akil et al. (2012). A fixed
20 volume (2 μ l) of a solution containing AAV8-*Pjvk* or AAV2/8-*Pjvk*-IRES-EGFP
21 recombinant viruses (10^{13} viral genomes/ml) was gently injected into the perilymphatic
22 compartment of the cochlea through the round window. The pipette was withdrawn, the
23 round window niche was quickly sealed with fascia and adipose tissue, and the bulla was
24 sealed with adhesive tape (3M Vetbond).

25

1 **Anti-oxidant treatment**

2 All anti-oxidant drugs were purchased from Sigma. A dose of 1% N-acetyl-cysteine, or a
3 cocktail of 0.75% α -lipoic acid, 0.5% α -tocopherol and 1% N-acetyl-cysteine, was added to
4 the drinking water of *Pjvk*^{-/-} mice during and after pregnancy, such that that the *Pjvk*^{-/-} pups
5 received the drug first in utero, and then via breast milk until P21. The auditory function of
6 the pups, raised in groups of four pups per cage, was tested on P21.

7

8 **Immunofluorescence studies**

9 For the detection of lipid oxidation products in the cochlea by immunohistofluorescence,
10 inner ears were dissected in phosphate-buffered saline (PBS) and fixed by immersion in 4%
11 paraformaldehyde (PFA) in PBS for 2 hours at 4°C. The samples were decalcified by
12 incubation in 10% EDTA in PBS, pH 7.4, for 4 days at 4°C, fixed again in 4% PFA in PBS
13 for 1 hour, rinsed twice in PBS for 10 minutes each, and immersed in 20% sucrose in PBS
14 for 12 hours. They were embedded in Tissue Freezing Medium (Triangle Biomedical
15 Sciences) and frozen. Cryostat sections (12 μ m thick) were used for
16 immunohistofluorescence, with an antibody against 4-hydroxy-2-nonenal (1:200, Abcam
17 ab46545).

18 For brainstem immunohistofluorescence analyses, P21 mice were killed by the injection of a
19 lethal dose of ketamine chlorhydrate, and perfused intravascularly with PBS, followed by
20 4% PFA in PBS. The brain was excised and fixed in 4% PFA in PBS for 1 hour at 4 °C. The
21 fixed tissues were immersed in 20% sucrose at 4°C overnight, and then frozen in dry ice-
22 cooled isopentane at -30°C to -50°C. Cryostat sections (14 μ m thick) were cut and used for
23 immunohistofluorescence analyses.

24 For whole-mount immunolabeling analyses, the inner ears were fixed in 4% PFA in PBS,
25 and the cochlear sensory areas (organ of Corti) were microdissected. The tissues were rinsed

1 twice in PBS, then permeabilized and blocked by incubation in PBS containing 20% normal
2 goat serum and 0.3% Triton X-100 for 1 hour at room temperature. For GFP detection,
3 whole-mount cochleas were incubated with a mixture of rabbit anti-GFP antibody (1:100,
4 Invitrogen A11122) and chicken anti-GFP antibody (1:100, Abcam ab13970) in 1% bovine
5 serum albumin (BSA) in PBS. A monoclonal antibody against parvalbumin (1:500, Sigma
6 SAB4200545) was used to label auditory neurons. A polyclonal antibody against
7 peroxisome membrane protein 70 (PMP70, 1:100, Abcam ab3421) was used to label
8 peroxisomes. Anti-myosin VI (Roux et al., 2009), anti-ribeye/CtBP2 (Santa Cruz sc-5966),
9 and anti-glutamate receptor 2 (GluR2, Invitrogen 32-0300) antibodies were used to delimit
10 the contours of IHCs, to label and count IHC ribbons, and to label post-synaptic glutamate
11 receptors on the dendritic ends of cochlear ganglion neurons, respectively.

12 For immunocytofluorescence analyses, HeLa and HepG2 cells were fixed by incubation in
13 4% PFA in PBS for 15 minutes, washed in PBS, and incubated in 50 mM NH₄Cl, 0.2%
14 Triton X-100 solution for 15 minutes at room temperature. The cells were washed and
15 incubated in 20% normal goat serum in PBS for 1 hour. Cells were incubated with the
16 primary antibody in 1% BSA in PBS for 1 hour. Peroxisomes were labeled with an antibody
17 against PMP70 (1:100, Abcam ab3421). An antibody against mitochondrial import receptor
18 subunit TOMM22 (1:100, Sigma HPA003037) was used to label mitochondria. The mouse
19 monoclonal antibody against pejvakin (Pjvk-G21) was used at 100 µg/ml to determine the
20 subcellular distribution of pejvakin. Cells were then washed in PBS and incubated with the
21 appropriate secondary antibody for 1 hour at room temperature.

22 For immunofluorescence studies, we used Atto-488- or Atto-647-conjugated goat anti-rabbit
23 IgG (1:500, Sigma 18772, 40839), Atto-550-conjugated goat anti-mouse IgG (1:500, Sigma
24 43394) and Alexa-Fluor-488-conjugated goat anti-chicken IgG (1:500, Invitrogen A11039)
25 as secondary antibodies. Atto-565 phalloidin (1:700, Sigma 94072) and DAPI (1:7500,

1 Sigma D9542) were used to label actin and cell nuclei, respectively. Images were acquired
2 with a Zeiss LSM700 Meta confocal microscope (Carl Zeiss MicroImaging, Inc.).
3 Peroxisomes were counted automatically with the Particles Analysis plugin of ImageJ
4 software (Collins, 2007). Enlarged peroxisomes were identified by measurements in two
5 perpendicular directions, with ImageJ software.

6

7 **Morphological analyses and peroxisome staining**

8 For scanning electron microscopy studies, mouse inner ears from P15 and P30 mice were
9 fixed by perfusion of the perilymphatic compartment with 2.5% phosphate-buffered
10 glutaraldehyde, and rinsed in PBS. Cochleas were then microdissected, dehydrated in graded
11 ethanol solutions, and dried to critical point. Processed specimens were then mounted on
12 aluminum stubs with colloidal silver adhesive and sputter-coated with gold palladium before
13 imaging in a JSM-6700 F Jeol scanning electron microscope. Inner ears from 10 *Pjvk*^{+/+}
14 mice (three at P15, four at P30, and three at P60), and 12 *Pjvk*^{-/-} mice (three at P15, five at
15 P30, and four at P60) were analyzed.

16 For transmission electron microscopy studies, cochleas were prepared as previously
17 described (Thelen et al., 2009). They were fixed by incubation in 2.5% glutaraldehyde in 0.1
18 M Sørensen's buffer, pH 7.4, for 2 hours at 4°C. After several washes in 0.1 M Sørensen's
19 buffer (pH 7.4), the samples were postfixed by incubation at 4°C with 2% osmium tetroxide
20 in the same buffer for 1 hour. The selective staining of peroxisomes was carried out by a
21 modified version of a published method (Angermüller & Fahimi, 1981). Briefly, the
22 cochleas were fixed by incubation in 1% glutaraldehyde in 0.1 M cacodylate buffer, pH 7.2,
23 at 4°C for 1 hour. After several washes in this buffer, the samples were immersed in 10 mM
24 3,3'-diaminobenzidine (DAB) and 0.15% H₂O₂ in 0.05 M Teorell-Stenhagen buffer (57
25 mM boric acid, 50 mM phosphoric acid, 35 mM citric acid, 345 mM NaOH), pH 10.5, for

1 45 minutes at 30°C. After several washes in the same buffer, the samples were postfixed by
2 incubation with 2% osmium tetroxide in H₂O for 1 hour at 4°C. All the cochleas were then
3 washed in deionized water, dehydrated in graded ethanol solutions, and embedded in Epon
4 (Epon-812, Electron Microscopy Sciences) for 48 hours at 60°C.

5 Ultrathin sections (70 nm thick) were obtained with an ultramicrotome (Reichert Ultracut E)
6 equipped with a diamond knife (Diatome). The sections were mounted on copper grids
7 coated with collodion. Sections for morphological analysis were contrast-stained with uranyl
8 acetate and lead citrate, for 15 minutes each. The ultrathin sections were observed under a
9 JEM-1400 transmission electron microscope (Jeol) at 80 kV and photographed with an 11
10 MegaPixel bottom-mounted TEM camera system (Quemesa, Olympus). The images were
11 analyzed with iTEM software (Olympus). The quantitative data were obtained with the same
12 software.

13

14 **Acoustic exposure for the quantification of cochlear transcripts and peroxisomes**

15 Three-week-old C57Bl/6 wild-type mice were used. In the first set of experiments, the
16 animals were exposed to overstimulation for one hour with bandpass-filtered white noise,
17 the spectrum of which covered the 5-20 kHz interval with an intensity of 105 dB SPL. Both
18 transcripts and peroxisomes were quantified. In the second set of experiments, in which only
19 transcripts were quantified, the mice were subjected to bandpass-filtered white noise with a
20 spectrum covering the 5-20 kHz interval, but a lower intensity (90 dB SPL), for 1 hour. The
21 white noise signal was generated with in-house Matlab software (The Mathworks), and was
22 delivered by an amplifier to a set of four Ultrasonic Vifa speakers (Avisoft Bioacoustics).
23 The speakers were attached to the tops of four custom-made, cylindrical sound-isolation
24 chambers (15 cm in radius), in which the mice were enclosed. The noise intensity delivered
25 by the speakers was calibrated with a BK4812 probe (Bruel & Kjaer) placed centrally on the

1 lower surface of the isolation chambers. The sound field within each chamber varied by less
2 than 10 dB over the lower surface.

3

4 **Microarray analysis and quantitative RT-PCR**

5 Total RNA was extracted from dissected organs of Corti from *Pjvk*^{-/-} and wild-type (*Pjvk*^{+/+})
6 P15 mice in Trizol reagent (Invitrogen), purified on RNeasy columns (Qiagen), and tested
7 on an Agilent (Waldbronn) 2100 Bioanalyzer. Three biological replicates were run for each
8 genotype. The cRNAs obtained from 100 ng of RNA were amplified with the GeneChip
9 Expression Two-Cycle 3' amplification system (Affymetrix). Fragmented biotin-labeled
10 cRNA samples were hybridized to Affymetrix Mouse Gene ST 1.0 arrays. The array was
11 then washed and stained according to the Affymetrix protocol. The stained array was
12 scanned at 532 nm with an Affymetrix GeneChip Scanner 3000, producing CEL files. Gene
13 expression levels were estimated from the CEL file probe-level hybridization intensities
14 with the model-based Robust Multichip Average algorithm (Bolstad et al. 2003). Arrays
15 were compared in local pool error tests (Jain et al., 2003), and the p values were adjusted
16 with the Benjamini–Hochberg algorithm (Benjamini & Hochberg, 1995). The fold
17 differences reflect the relative expression levels of the genes in the organs of Corti of *Pjvk*^{-/-}
18 mice normalized with respect to *Pjvk*^{+/+} mice.

19 The differences in *Mpv17*, *c-Dct*, *Gpx2*, *CypA*, *c-Fos*, and *Hsp70* transcript levels between
20 sound-exposed and unexposed cochleas were analyzed by quantitative RT-PCR. For sound-
21 exposed mice, cochleas were collected at 1 hour, 3 hours, 6 hours, and 18 hours after sound-
22 exposure. RNA was extracted from dissected organs of Corti, with the NucleoSpin[®] RNA II
23 kit (Macherey-Nagel). Quantitative RT-PCR was performed with the Universal Probe
24 Library (UPL) system from Roche. UPL probes were labeled with a fluorescein derivative
25 (FAM), and the fluorescence was read with the Applied Biosystems 7500 Real-Time PCR

1 System. The thermocycling conditions were 50°C for 2 minutes, followed by 95°C for 2
2 minutes, and then 40 cycles of 95°C for 15 s and 60°C for 30 s. Three independent
3 experiments were performed for each sound-exposed or unexposed cochlea. Each assay was
4 conducted for the target transcript probe-set in a multiplex reaction in which the
5 glyceraldehyde-3-phosphate dehydrogenase (*Gapdh*) probe set was used as an internal
6 control. Relative levels of target transcripts were determined by the comparative cycle
7 threshold (CT) method. The relative copy number for each target transcript was calculated as
8 $2^{-\Delta\Delta CT}$. The sequences of the primers and UPL probes are available on request.

9 Transcription levels in the organ of Corti were compared, for each gene, between sound-
10 exposed and unexposed mice, in unpaired Student's *t*-tests.

11

12 **Measurements of synaptic exocytosis and $I_{K,f}$ (BK) current in IHCs, and non-linear** 13 **capacitance in OHCs**

14 Experiments were carried out on explants of the organ of Corti. The dissecting-steps were
15 performed in a cold (5-10°C) perilymph-like solution containing (in mM): 135 NaCl, 5.8
16 KCl, 1.3 CaCl₂, 0.9 MgCl₂, 0.7 NaH₂PO₄, 5.6 D-glucose 2 Na pyruvate and 10 Na-HEPES;
17 pH 7.4 and osmolality near 300 mosmol/kg. The freshly dissected sensory organ was then
18 mounted flat and continuously perfused at room temperature (22-24°C) in a perilymph-like
19 solution. The sensory hair cells were viewed through a X40 LWD water immersion
20 objective (NA = 0.8) on an Olympus BX51WI microscope. Whole-cell voltage clamp
21 recordings were obtained using 3-4 MW electrodes pulled from borosilicate glass
22 capillaries (1B150F-4, WPI Sarasota Fl) on a Sachs-Flaming Microelectropuller (Model PC-
23 84, Sutter Instrument Company). Acquisition was done using the Patchmaster software
24 (HEKA).

25 Ca²⁺ current and exocytosis recordings in IHCs were performed in the perilymph-like

1 solution containing 5 mM Ca^{2+} and supplemented with 1 μM TTX (Sigma), 10 mM TEA-Cl
2 and 100 nM apamin (Latoxan). The internal pipette solution contained the following (in
3 mM): 150 CsCl, 1 MgCl_2 , 5 TEA-Cl, 1 EGTA, 5 Na_2ATP , 0.5 Na_2GTP , 5 Cs-HEPES; pH
4 7.4 and osmolality near 300 mosmol/kg. The liquid junction potential was about 2 mV and
5 was not corrected in our C_m experiments. Real time changes in membrane capacitance (ΔC_m)
6 were measured using the “track-in” circuitry the HEKA EPC 10 patch clamp amplifier as
7 previously described (Dulon et al., 2009). A 2.5 kHz sine wave of 15-20 mV was applied to
8 the cells from a holding potential of -80 mV. C_m signals were low-pass filtered at 80 Hz.
9 ΔC_m responses were measured 50 ms after the end of the depolarizing pulse, and averaged
10 over a period of 100 to 300 ms.

11 For BK current measurement in IHCs, IHCs were bathed in the perilymph-like solution. The
12 internal solution was a 290 mOsm KCl-based internal solution containing (in mM): 135
13 KCl, 0.1 CaCl_2 , 1.5 $\text{MgCl}_2 \cdot 6\text{H}_2\text{O}$, 11 EGTA, 5 HEPES, 2.5 Na_2ATP ; pH 7.4. Series
14 resistance compensation (50-65%; $R_s = 6.34 \pm 0.34 \text{ M}\Omega$) was applied on line with the series
15 resistance compensation circuitry of the amplifier throughout recordings. To construct the
16 current-voltage curves, $I_{K,f}$ current amplitude were measured at 1.3 ms after the start of
17 voltage-pulse (from a holding potential of -80 mV) and at the end of the depolarization step.
18 Paxilline, 4-aminopyridine, and XE991, blockers of $I_{K,f}$, $I_{K,s}$, and $I_{K,n}$ currents, respectively,
19 were added to the external solution when necessary.

20 Nonlinear capacitance measurements were performed as described previously (Beurg et al.,
21 2013).

22

23 **Imaging of mitochondrial membrane potential in a hemicochlea preparation**

24 We used the hemicochlea preparation described by Dallos and coworkers (Teudt and
25 Richter, 2007). Briefly, P17- P30 mice were lightly anaesthetized with isoflurane gas and

1 decapitated. The cranium was cut in half along the median sagittal axis. The temporal bones
2 were removed and fixed to the stage of a vibrating tissue cutter (Vibratome 3000) with
3 cyanoacrilate glue. Cochleas were then cut in half along the mid modiolar plane with a
4 microtome blade (R35 Feather, Osaka, Japan) under ice-cold modified perilymph (22.5 mM
5 NaCl, 120 mM sodium gluconate, 3.5 mM KCl, 1 mM CaCl₂, 1 mM MgCl₂, 10 mM
6 HEPES, 5.5 mM glucose). The pH was adjusted to 7.3-7.4, and the solution was saturated
7 with 100 % O₂. The upper half of the cochlea was discarded after cutting. Only the lower
8 parts were used for experiments.

9 For functional imaging of mitochondrial membrane potential ($\Delta\psi_m$), the hemicochleas were
10 loaded with 5 μ M rhodamine 123 (Rh123, Invitrogen) for 5 minutes at room temperature,
11 then washed. When Rh123 is used in the quenched mode, mitochondrial depolarization
12 produces a marked increase in the fluorescence, and $\Delta\psi_m$ changes can be followed reliably
13 (Nicholls and Ward, 2000; Duchen et al., 2003). A perfusion of the protonophore carbonyl
14 cyanide 4-(trifluoromethoxy)phenylhydrazone (FCCP, Sigma) at a concentration of (2 μ M)
15 was used to trigger $\Delta\psi_m$ collapse.

16 Hemicochleas were continuously perfused with modified perilymph in an experimental
17 chamber. The perfusion velocity was 3.5 ml/minute, and the solution was 100 % saturated
18 with O₂. All experiments were performed at 36 ± 0.5 °C. Fluorescent images were obtained
19 with an upright epifluorescent microscope (Olympus BX50WI) equipped with a 4x objective
20 (Olympus XLFluor 4x/340 NA 0.28). With this set up, we were able to image the entire
21 hemicochlea preparation. Oblique illumination was used for orientation purposes. Changes
22 in $\Delta\psi_m$ were observed over the whole section of the cochlear ganglion and organ of Corti in
23 the basal, middle and apical cochlear turns. Rh123 was excited at 495 ± 5 nm with a
24 monochromator equipped with a xenon arc lamp (Polychrome II; T.I.L.L. Photonics
25 GMBH). Emitted light was filtered by a 535/50 band-pass filter (Chroma Technology

1 Corporation) and detected with a cooled CCD camera (Photometrics Quantix), at an image
2 frame rate of 12 images/minute. Image intensities were background-corrected using a nearby
3 area devoid of loaded cells. Axon Imaging Workbench 6 software (Axon Instruments) was
4 used for image acquisition and detailed offline analysis. The data were further analyzed and
5 plotted with Wavemetrics Igor Pro 6. The rise time of the evoked mitochondrial
6 depolarization was determined as the time needed from the start of the response to
7 maximum intensity.

8

9 SUPPLEMENTAL FIGURE LEGENDS

10 **Figure S1. Strategy for the targeted replacement of the *Pjvk* wild-type allele with a**
11 **floxed allele.** (A) Schematic diagram of the murine *Pjvk* gene and the targeting construct
12 used to produce a floxed *Pjvk* allele (*Pjvk*^{fl}) with loxP sequences (triangles) flanking exon 2,
13 followed by a *PGK-neo* cassette. *DTA*: diphtheria toxin A fragment. An additional *SacI* site
14 (in bold) was engineered after the first loxP site, for Southern blot analysis. Small arrows
15 indicate the positions of the PCR primers used to screen for clones of recombinant
16 embryonic stem cells. Right panel: Southern blot analysis of *SacI*-digested genomic DNA
17 from *Pjvk*^{+/+} (+/+) and *Pjvk*^{fl/+} (fl/+) mice. Exon 2 of *Prkra* (a gene flanking *Pjvk*, on the
18 centromeric side) was used as the probe for Southern blot analysis. The probe hybridizes to a
19 4.6 kb fragment from the floxed allele and a 7.2 kb fragment from the wild-type allele. (B)
20 RT-PCR analysis of the *Pjvk* transcript in the inner ears of *Pjvk*^{+/+} and *Pjvk*^{-/-} P7 mice. *Pjvk*^{-/-}
21 mice were obtained by crossing *Pjvk*^{fl/fl} mice with transgenic mice carrying the cre
22 recombinase gene under the control of the ubiquitous *PGK* promoter. The expected 1059 bp
23 amplicon was detected in the *Pjvk*^{+/+} mouse (lane 1), whereas a 963 bp fragment was
24 detected in the *Pjvk*^{-/-} mouse (lane 2), because of the deletion of exon 2. M, DNA size
25 marker: φX174 DNA *HaeIII* digest.

1

2 **Figure S2. Transduction of neurons in the auditory pathway and of cochlear hair cells**
3 **with the AAV8 and AAV2/8 viral vectors, respectively.** AAV8-EGFP or AAV2/8-EGFP
4 was injected into the cochleas of P3 mice, and transduced cells were detected at P21 by
5 EGFP immunostaining (green) on cryosections of the cochlear ganglion (basal turn) (A,
6 lower panel) and of the cochlear nucleus (A, upper panel), and whole-mount preparations of
7 the organ of Corti from the cochlear middle turn (B). The block diagram shows the organ of
8 Corti and the main ascending auditory pathway that projects both ipsilaterally and
9 contralaterally (for the sake of clarity, we show projections from only one cochlea). AAV8-
10 EGFP-transduced auditory neurons are identified by their parvalbumin (red) and EGFP
11 (green) co-immunoreactivity (A). AAV2/8-EGFP transduces the vast majority of inner hair
12 cells (IHCs) and a smaller proportion of outer hair cells (OHCs). The numbers on the DAPI-
13 stained cell nuclei indicate the three rows of OHCs (B). Scale bars are 50 μm in (A) and 10
14 μm in (B).

15

16 **Figure S3. (A) Progressive degeneration of the organ of Corti in *Pjvk*^{-/-} mice.** Upper
17 panels: Scanning electron micrographs showing surface views of the organ of Corti in the
18 basal turn of the cochlea from P60 *Pjvk*^{+/+} and *Pjvk*^{-/-} mice. In the *Pjvk*^{-/-} mouse, many outer
19 hair cells (OHCs), inner hair cells (IHCs), and pillar cells (PCs) are missing. Scale bars are 5
20 μm . Lower panels: Light micrographs of cross sections taken from the middle turn of the
21 cochlea in *Pjvk*^{+/+} and *Pjvk*^{-/-} mice at P90. In the *Pjvk*^{-/-} mouse, all OHCs, IHCs, and
22 supporting cells have degenerated and the organ of Corti is collapsed (arrow). In addition,
23 the numbers of nerve fibers and cochlear ganglion neurons (arrowheads) are markedly
24 decreased. Scale bars are 80 μm . **(B) Increased lipid peroxidation in the cochlea of *Pjvk*^{-/-}**
25 **mice.** Cryosections of the organ of Corti (middle turn, upper panels) and of the cochlear

1 ganglion (apical and basal turns, lower panels) from P60 *Pjvk*^{+/+} and *Pjvk*^{-/-} mice,
2 immunolabeled for 4-HNE, a by-product of lipid peroxidation (green), and stained with
3 DAPI (blue) to show cell nuclei. Asterisks indicate the nuclei of OHCs and IHCs. In the
4 *Pjvk*^{-/-} mouse, some OHCs and cochlear ganglion neurons are missing, but the OHCs present
5 are highly immunoreactive for 4-HNE (arrows), as are the cochlear ganglion neurons,
6 especially in the basal turn. Scale bars are 20 μm.

7

8 **Figure S4. (A) Quantitative RT-PCR in *Pjvk*^{-/-} mice to confirm microarray results for**
9 **the genes involved in redox balance.** "Fold change" denotes the level of expression of the
10 gene in the organ of Corti of *Pjvk*^{-/-} mice relative to that in *Pjvk*^{+/+} mice, with the minus sign
11 indicating downregulation. All four genes tested, *c-Dct*, *Mpv17*, *CypA*, and *Gpx2*, were less
12 strongly expressed in the organ of Corti of P15 *Pjvk*^{-/-} mice than in *Pjvk*^{+/+} mice, in both
13 microarray (transcriptome) and quantitative RT-PCR (qRT-PCR) analyses. **(B) Effect of**
14 **exposure of wild-type (*Pjvk*^{+/+}) mice to loud sound on the expression of *Pjvk* and other**
15 **anti-oxidant genes in the organ of Corti.** Relative levels (fold change) of *Pjvk*, *c-Dct*,
16 *CypA*, *c-Fos*, and *HSP70* transcripts, as measured by quantitative RT-PCR in the organ of
17 Corti of sound-exposed (5-20 kHz, 90 dB for 1 hour) P21 wild-type (*Pjvk*^{+/+}) mice after 6
18 hours in a silent environment versus levels in unexposed mice. Sound-exposure leads to a
19 marked increase in the levels of *Pjvk* and *CypA* transcripts (3.0 ± 0.3-fold and 4.0 ± 1.0-fold,
20 respectively), but only a moderate (less than 2-fold) increase in the levels of *c-Dct*, *Hsp70*,
21 and *c-Fos* transcripts. This indicates that *Pjvk* and *CypA* are involved in the early cochlear
22 response to noise. Error bars indicate the SEM.

23 **Figure S5. (A) Pejvakin is associated with peroxisomes in transfected HeLa cells.**
24 Transfected HeLa cells producing pejvakin (*Pjvk*-EGFP, upper panel) and untransfected
25 cells (lower panel) were immunostained with both an anti-pejvakin antibody (*Pjvk*-G21) and

1 an antibody against peroxisome membrane protein 70 (PMP70). Cell nuclei were stained
2 with DAPI (blue). Colocalization of the immunostainings of pejkakin (red) and PMP70
3 (green) was observed in transfected cells (see inset for higher magnification of the boxed
4 area). Pejkakin was not detected in untransfected cells. **(B) Absence of immunolabeling in
5 inner hair cells (IHCs) from P21 *Pjvk*^{-/-} and *Pjvk*^{fl/fl} *Myo15-cre*^{+/-} mice with the Pjvk-
6 G21 antibody** demonstrates the specificity of this antibody (see Figure 5B for
7 immunolabeling in *Pjvk*^{+/+} IHCs). **(C) Pejkakin immunostaining of dividing peroxisomes.**
8 Double immunolabeling of HepG2 cells for pejkakin (red) and PMP70 (green). Upper panel:
9 arrowheads indicate pejkakin-immunoreactive protrusions from pre-existing peroxisomes.
10 Lower panel: boxed areas show pejkakin-immunoreactive string-of-beads structures
11 corresponding to elongated and constricted peroxisomes (preceding final fission) are boxed.
12 Scale bar is 10 μm in (A), 5 μm in (B), and 2 μm in (C).

13

14 **Figure S6. (A) Proliferation of peroxisomes induced by H₂O₂ in *Pjvk*^{+/+} mouse
15 embryonic fibroblasts.** F-actin (red), PMP70 (green), and DAPI (blue) staining of *Pjvk*^{+/+}
16 (left panel) and *Pjvk*^{-/-} (right panel) mouse embryonic fibroblasts (MEFs), treated with 0.5
17 mM H₂O₂ for 4 hours or left untreated, and analyzed 18 hours later. H₂O₂-treatment
18 increases the number of peroxisomes only in the *Pjvk*^{+/+} cells (see quantification in Figure
19 5C). **(B) Larger numbers and enlargement of peroxisomes in transfected HeLa cells
20 producing wild-type and mutant forms of pejkakin, respectively.** In untransfected cells
21 (NT) and in cells producing EGFP alone, EGFP and wild-type pejkakin (*Pjvk*), or EGFP and
22 the p.T54I, p.R183W, p.C343S, or p.V330Lfs*7 mutated forms of pejkakin, peroxisomes
23 were identified on the basis of their PMP70-immunoreactivity. The upper panel shows F-
24 actin (red), DAPI (dark blue), EGFP (green), and PMP70 (light blue) staining, whereas the
25 lower panel shows only the PMP70 immunostaining of individual cells delimited by a white

1 border. The number of peroxisomes is larger in cells producing wild-type pejevakin, and
2 smaller in the cells producing any of the mutated forms of pejevakin, than in cells producing
3 EGFP alone (see quantification in Figure 5D). In addition, cells producing the mutated
4 forms of pejevakin contain enlarged peroxisomes (arrowheads, and see insets for
5 magnification; see also quantification in Figure 5D). Scale bar is 20 μm in (A) and 10 μm in
6 (B).

7

8 **Figure S7. (A) Normal number of ribbon synapses and Ca^{2+} -dependent synaptic**
9 **exocytosis in *Pjvk*^{-/-} inner hair cells (IHCs).** Upper panel : The synapses between IHCs and
10 the primary auditory neurons were double-immunolabeled for the presynaptic marker ribeye
11 that labels IHC ribbons (green), and the postsynaptic glutamate receptor GluR2 (red). The
12 bar chart shows the quantitative analysis of ribbon synapses from *Pjvk*^{+/+} (blue) and *Pjvk*^{-/-}
13 (red) mice on P20. N: cell nucleus of IHCs. Lower panel: Synaptic function. Left: Bar chart
14 representation of the peak of I_{Ca} and of the increase in membrane capacitance (ΔC_{m}) in
15 response to a 100 ms voltage step from -80 mV to -10 mV in *Pjvk*^{+/+} (blue) and *Pjvk*^{-/-} (red)
16 P20 IHCs. I_{Ca} and ΔC_{m} values were similar in *Pjvk*^{-/-} IHCs (126 ± 16 pA and 21.3 ± 2.2 fF, n
17 = 6) and *Pjvk*^{+/+} IHCs (110 ± 16 pA and 20.0 ± 2.0 fF, $n = 5$; t-test, $p = 0.47$ and $p = 0.64$).
18 Middle: Synaptic transfer function describing the relation between ΔC_{m} and I_{Ca} in *Pjvk*^{+/+} (n
19 = 3; blue dots) and *Pjvk*^{-/-} ($n = 3$; red dots) P20 IHCs. Cells were stimulated by a constant
20 100 ms voltage step at various membrane potentials from -80 mV to -5 mV. Fits to single
21 data points were done by using a simple power function with $N = 0.70 \pm 0.10$ and $N = 0.63 \pm$
22 0.10 in *Pjvk*^{-/-} and *Pjvk*^{+/+} IHCs, respectively. The mean slope representing Ca^{2+} efficiency
23 was 0.17 ± 0.05 and 0.15 ± 0.02 fF/pA in *Pjvk*^{-/-} IHCs and *Pjvk*^{+/+} IHCs, respectively (t -test,
24 $p = 0.73$). Right: Increase in membrane capacitance (ΔC_{m}) produced by a train of 20
25 successive 100 ms voltage steps from -80 to -10 mV, separated by 100 ms time intervals, in

1 *Pjvk*^{+/+} (n = 3; blue dots) and *Pjvk*^{-/-} (n = 3; red dots) P20 IHCs. *Pjvk*^{-/-} and *Pjvk*^{+/+} IHCs
2 display similar linear increase in membrane capacitance (mean slope of 5.14 ± 0.10 and 5.04
3 ± 0.35 fF/stimulus in *Pjvk*^{-/-} and *Pjvk*^{+/+} mice, respectively; t-test, p = 0.76).

4 **(B) Most *Pjvk*^{-/-} inner hair cells (IHCs) lack the fast voltage-activated $I_{K,f}$ current.** $I_{K,f}$,
5 $I_{K,s}$, and $I_{K,n}$ are the main K⁺ currents found in mature IHCs. Upper left: Example traces for
6 potassium currents ($I_{K,f} + I_{K,s}$) recorded for a voltage step to -10 mV from a holding potential
7 of -80 mV, in a P19 *Pjvk*^{+/+} (blue) and two P19 *Pjvk*^{-/-} (red) IHCs. Enlarged time scale of the
8 current onset, on the right, shows the fast voltage-activated outward current, $I_{K,f}$, in the
9 control IHC and one *Pjvk*^{-/-} IHC, whereas in the other *Pjvk*^{-/-} IHC, only a slow current can be
10 observed. Upper middle: Current-voltage (*I-V*) curves representing mean amplitudes of $I_{K,f}$
11 (measured 1.3 ms after the onset of the depolarizing pulse, a time point at which $I_{K,s}$ is not
12 yet activated) and of the steady-state current ($I_{K,f} + I_{K,s}$, measured at the end of the voltage
13 step) as a function of the membrane potential (V_m). For *Pjvk*^{-/-} IHCs, two cell groups were
14 defined, based on the presence (open circles) or absence (closed circles) of $I_{K,f}$. Upper right:
15 bar charts showing the mean amplitudes of the $I_{K,f}$ and $I_{K,f} + I_{K,s}$ currents obtained in
16 response to a voltage-step from -80 to -10 mV. $I_{K,f}$ was detected in all 7 IHCs from *Pjvk*^{+/+}
17 mice, but in only four of the 11 IHCs from *Pjvk*^{-/-} mice. The current-voltage relationship at
18 1.3 ms did not display significantly different conductances in *Pjvk*^{+/+} IHCs (160 ± 20 nS, n =
19 7) and in the few *Pjvk*^{-/-} IHCs showing $I_{K,f}$ (129 ± 25 nS, n = 4 out of 11), with a mean $I_{K,f}$
20 amplitude at -10 mV of 1.2 ± 0.2 nA and 0.9 ± 0.3 nA, respectively (p = 0.53 for both
21 conductance and amplitude comparisons). Lower left: $I_{K,f}$ blockade with paxilline (10 μ M), a
22 selective BK channel blocker, in *Pjvk*^{+/+} and *Pjvk*^{-/-} IHCs submitted to a voltage step from -
23 80 to -10 mV. No current reduction in the presence of paxilline (both at 1.3 ms and steady
24 state plateau) was observed in the *Pjvk*^{-/-} IHCs that displayed only the slow outward current
25 component $I_{K,s}$, indicating that these cells indeed do not have functional BK channels. The

1 amplitudes of $I_{K,s}$ were similar in $Pjvk^{+/+}$ and $Pjvk^{-/-}$ IHCs (1.76 ± 0.41 nA vs. 1.65 ± 0.24
2 nA at -10 mV; t -test, $p = 0.6$). Lower middle: Traces representing potassium currents ($I_{K,f} +$
3 $I_{K,s} + I_{K,n}$) in an IHC from a P19 $Pjvk^{-/-}$ mouse. Lower right: Bar chart showing the mean
4 amplitudes of $I_{K,n}$ measured at -120 mV in IHCs from P19 $Pjvk^{-/-}$ and $Pjvk^{+/+}$ mice. Inward
5 $I_{K,n}$ currents, sensitive to XE991 (2 μ M; data not shown), were recorded in all P19-P24
6 $Pjvk^{+/+}$ and $Pjvk^{-/-}$ IHCs in response to hyperpolarizing voltage steps from -80 mV to -120
7 mV, and their amplitudes were similar in the two groups (0.93 ± 0.13 nA vs. 1.3 ± 0.28 nA,
8 respectively; $n = 6$ in both groups; t -test, $p = 0.3$). Together, these results indicate that $Pjvk^{-/-}$
9 IHCs display normal $I_{K,s}$ and $I_{K,n}$ currents, but most of the cells (64 % of the $Pjvk^{-/-}$ IHCs
10 tested) lack the $I_{K,f}$ (BK) current.

11 **(C) Impaired electromotility of $Pjvk^{-/-}$ OHCs.** Left panel: Non-linear capacitance ($C_{\text{non-}}$
12 linear) of 10 $Pjvk^{+/+}$ and 16 $Pjvk^{-/-}$ OHCs, as a function of the membrane potential (V_m).
13 Smooth lines are fits based on a two-state Boltzmann function (implemented in JClamp)
14 with values of Q_{max} , $V_{1/2}$, z , and C_{linear} of: 1.1 ± 0.9 pC, -33.6 ± 3.5 mV, 0.75 ± 0.05 , and 6.6
15 ± 0.2 pF for $Pjvk^{+/+}$ OHCs, and 0.83 ± 0.37 pC, -30.5 ± 1.3 mV, 0.85 ± 0.03 , 7 ± 0.3 pF for
16 $Pjvk^{-/-}$ OHCs. Right panel: Bar charts showing a 30% decrease of maximal charge density in
17 $Pjvk^{-/-}$ OHCs.

18 **(D) Dissipation of the $\Delta\psi_m$ revealed no difference in mitochondrial status between**
19 **$Pjvk^{+/+}$ and $Pjvk^{-/-}$ cochleas.** Functional imaging of $\Delta\psi_m$ was performed over sections of
20 the organ of Corti and cochlear ganglion, in turns of the hemicochlea of P17-P30 mice,
21 after loading the preparation by Rh123. A perfusion of the protonophore FCCP was used to
22 trigger $\Delta\psi_m$ collapse. The starting latencies (SL) of the response and rise times (RT) of the
23 evoked depolarization peaks were calculated and compared. The inset graphs demonstrate
24 the way of determination of SL and RT on a representative trace. In the bar charts, basal,
25 middle, and apical denote cochlear turns. The six regions of interest are delimited by black

1 border on the insets showing the fluorescent and obliquely illuminated images of a
2 hemicochlea. Error bars represent SEM (n = 12 ears for each genotype). n.s., not
3 significant, *** p < 0.001.

Table S1. Transcriptional changes in the organ of Corti of *Pjvk*^{-/-} mice

Gene (encoded protein)	Accession number	Fold change	Adjusted p-value	Probe set	References
Genes involved in ROS metabolism					
<i>Mpv17</i> (Mpv17, mitochondrial inner membrane protein)	NM_008622	-3.40	3.34E-22	10529091	Binder et al, 1999; Meyer zum Gottesberge, 2001; Spinazzola et al., 2006
<i>c-Dct</i> (c-Dopachrome tautomerase)	NM_010024	-3.28	9.95E-50	10422249	Michard et al., 2008a; Michard et al., 2008b
<i>CypA</i> (Cyclophilin A)	NM_008907	-2.15	1.78E-09	10545337	Lee et al., 2001; Ge et al., 2009
<i>Gpx2</i> (Glutathione peroxidase 2)	NM_030677	-1.59	4.87E-11	10401109	Evans and Halliwell, 1999
Genes with modified expression in tumors					
<i>Tax1bp3</i> (Tax1 (human T-cell leukemia virus type I) binding protein 3)	NM_029564	-2.88	2.16E-15	10378334	Kanamori et al., 2003
<i>Plunc</i> (Palate, lung, and nasal epithelium associated protein)	NM_011126	2.20	6.89E-10	10477475	Bingle et al., 2005; He et al., 2005; Benlloch et al., 2009
<i>Cd59a</i> (CD59a antigen)	NM_001111060	-2.13	1.78E-30	10474229	Madjd et al., 2003; Watson et al., 2006
<i>Pramel3</i> (Preferentially expressed antigen in melanoma-like 3)	NM_031390	-1.94	6.05E-04	10601790	Schenk et al., 2007
<i>Lrp1b</i> (Low density lipoprotein-related protein 1b)	NM_053011	1.82	3.21E-07	10482336	Sonoda et al., 2004; Nakagawa et al., 2006; Lu et al., 2010
Genes encoding putative cell growth inhibitors					
<i>Ifi44</i> (Interferon-induced protein 44)	NM_133871	-2.20	3.45E-12	10502791	Hallen et al., 2007; Kim et al., 2009
<i>Ifit3</i> (Interferon-induced protein with tetratricopeptide repeats 3)	NM_010501	-2.08	2.72E-10	10462618	
<i>Ifit1</i> (Interferon-induced protein with tetratricopeptide repeats 1)	NM_008331	-1.75	1.53E-07	10462623	
<i>Ifitm3</i> (Interferon induced transmembrane protein 3)	NM_025378	-1.60	1.42E-11	10569017	

Genes encoding ribosomal proteins					
<i>Rps13</i> (Ribosomal protein S13)	NM_026533	2.04	5.61E-08	10565434	Wool, 1996; Lai and Xu, 2007
<i>Rps23</i> (Ribosomal protein S23)	NM_024175	-1.92	1.06E-08	10491730	
<i>Rpl36</i> (Ribosomal protein L36)	BC086914	-1.74	2.57E-04	10394609	
Gene involved in ubiquitin proteolytic pathway					
<i>UbB</i> (Ubiquitin B)	NM_011664	-1.64	2.93E-07	10376864	Fischer et al., 2003; de Pril et al., 2010
Gene encoding a synaptic protein					
<i>a39-Takusan</i> (Alpha39-takusan)	EF651836	2.30	1.39E-07	10417411	Tu et al., 2007

Fold change reflects the expression level of the gene in the organ of Corti of *Pjvk*^{-/-} relative to *Pjvk*^{+/+} mice. + and - denote up-regulation and down-regulation, respectively. The p values were adjusted using the Benjamini-Hochberg algorithm.

SUPPLEMENTAL REFERENCES

- Akil, O., Seal, R.P., Burke, K., Wang, C., Alemi, A., During, M., Edwards, R.H., and Lustig, L.R. (2012). Restoration of hearing in the VGLUT3 knockout mouse using virally mediated gene therapy. *Neuron* 75, 283-293.
- Angermuller, S., and Fahimi, H.D. (1981). Selective cytochemical localization of peroxidase, cytochrome oxidase and catalase in rat liver with 3,3'-diaminobenzidine. *Histochemistry* 71, 33-44.
- Benjamini, Y., and Hochberg, Y. (1995). Controlling the false discovery rate: a practical and powerful approach to multiple testing. *J. Roy. Statist. Soc. Ser. B* 57, 289-300.
- Benlloch, S., Galbis-Caravajal, J.M., Alenda, C., Peiro, F.M., Sanchez-Ronco, M., Rodriguez-Paniagua, J.M., Baschwitz, B., Rojas, E., and Massuti, B. (2009). Expression of molecular markers in mediastinal nodes from resected stage I non-small-cell lung cancer (NSCLC): prognostic impact and potential role as markers of occult micrometastases. *Ann. Oncol.* 20, 91-97.
- Beurg, M., Tan, X., Fettiplace, R. (2013). A prestin motor in chicken auditory hair cells: active force generation in a nonmammalian species. *Neuron* 79, 69-81.
- Binder, C.J., Weiher, H., Exner, M., and Kerjaschki, D. (1999). Glomerular overproduction of oxygen radicals in Mpv17 gene-inactivated mice causes podocyte foot process flattening and proteinuria: A model of steroid-resistant nephrosis sensitive to radical scavenger therapy. *Am. J. Pathol.* 154, 1067-1075.
- Bingle, L., Cross, S.S., High, A.S., Wallace, W.A., Devine, D.A., Havard, S., Campos, M.A., and Bingle, C.D. (2005). *SPLUNC1 (PLUNC)* is expressed in glandular tissues of the respiratory tract and in lung tumours with a glandular phenotype. *J. Pathol.* 205, 491-497.
- Bolstad, B.M., Irizarry, R.A., Astrand, M., and Speed, T.P. (2003). A comparison of normalization methods for high density oligonucleotide array data based on variance and bias. *Bioinformatics* 19, 185-193.
- Caberlotto, E., Michel, V., Foucher, I., Bahloul, A., Goodyear, R.J., Pepermans, E., Michalski, N., Perfettini, I., Alegria-Prevot, O., Chardenoux, S., *et al.* (2011). Usher type 1G protein sans is a critical component of the tip-link complex, a structure controlling actin polymerization in stereocilia. *Proc. Natl. Acad. Sci. U.S.A.* 108, 5825-5830.
- Collins, T.J. (2007). ImageJ for microscopy. *BioTechniques* 43, 25-30.

de Pril, R., Hobo, B., van Tijn, P., Roos, R.A., van Leeuwen, F.W., and Fischer, D.F. (2010). Modest proteasomal inhibition by aberrant ubiquitin exacerbates aggregate formation in a Huntington disease mouse model. *Mol. Cell. Neurosci.* *43*, 281-286.

Duchen, M.R., Surin, A., and Jacobson, J. (2003). Imaging mitochondrial function in intact cells. *Methods Enzymol.* *361*, 353-389.

Dulon, D., Safieddine, S., Jones, S.M., Petit, C. (2009). Otoferlin is critical for a highly sensitive and linear calcium-dependent exocytosis at vestibular hair cell ribbon synapses. *J Neurosci.* *29*, 10474-87.

Ehret, G., and Riecke, S. (2002). Mice and humans perceive multiharmonic communication sounds in the same way. *Proc. Natl. Acad. Sci. U.S.A.* *99*, 479-482.

Evans, P., and Halliwell, B. (1999). Free radicals and hearing. Cause, consequence, and criteria. *Ann. N. Y. Acad. Sci.* *884*, 19-40.

Fischer, D.F., De Vos, R.A., Van Dijk, R., De Vrij, F.M., Proper, E.A., Sonnemans, M.A., Verhage, M.C., Sluijs, J.A., Hobo, B., Zouambia, M., *et al.* (2003). Disease-specific accumulation of mutant ubiquitin as a marker for proteasomal dysfunction in the brain. *FASEB J.* *17*, 2014-2024.

Ge, Y.S., Teng, W.Y., and Zhang, C.D. (2009). Protective effect of cyclophilin A against Alzheimer's amyloid beta-peptide (25-35)-induced oxidative stress in PC12 cells. *Chin. Med. J.* *122*, 716-724.

Hallen, L.C., Burki, Y., Ebeling, M., Broger, C., Siegrist, F., Oroszlan-Szovik, K., Bohrmann, B., Certa, U., and Foser, S. (2007). Antiproliferative activity of the human IFN-alpha-inducible protein IFI44. *J. Interferon Cytokine Res.* *27*, 675-680.

He, Y., Zhou, G., Zhai, Y., Dong, X., Lv, L., He, F., and Yao, K. (2005). Association of *PLUNC* gene polymorphisms with susceptibility to nasopharyngeal carcinoma in a Chinese population. *J. Med. Genet.* *42*, 172-176.

Henry, K.R. (1979). Auditory brainstem volume-conducted responses: origins in the laboratory mouse. *J. Am. Aud. Soc.* *4*, 173-178.

Jain, N., Thatte, J., Braciale, T., Ley, K., O'Connell, M., and Lee, J.K. (2003). Local-pooled-error test for identifying differentially expressed genes with a small number of replicated microarrays. *Bioinformatics* *19*, 1945-1951.

Kanamori, M., Sandy, P., Marzinotto, S., Benetti, R., Kai, C., Hayashizaki, Y., Schneider, C., and Suzuki, H. (2003). The PDZ protein tax-interacting protein-1 inhibits beta-catenin transcriptional activity and growth of colorectal cancer cells. *J. Biol. Chem.* *278*, 38758-38764.

Kim, K.S., Kang, K.W., Seu, Y.B., Baek, S.H., and Kim, J.R. (2009). Interferon-gamma induces cellular senescence through p53-dependent DNA damage signaling in human endothelial cells. *Mech. Ageing Dev.* *130*, 179-188.

Kress, C., Vandormael-Pournin, S., Baldacci, P., Cohen-Tannoudji, M., and Babinet, C. (1998). Nonpermissiveness for mouse embryonic stem (ES) cell derivation circumvented by a single backcross to 129/Sv strain: establishment of ES cell lines bearing the Omd conditional lethal mutation. *Mamm. Genome* *9*, 998-1001.

Lai, M.D., and Xu, J. (2007). Ribosomal proteins and colorectal cancer. *Curr. Genomics* *8*, 43-49.

Lallemand, Y., Luria, V., Haffner-Krausz, R., and Lonai, P. (1998). Maternally expressed PGK-Cre transgene as a tool for early and uniform activation of the Cre site-specific recombinase. *Transgenic Res.* *7*, 105-112.

Lee, S.P., Hwang, Y.S., Kim, Y.J., Kwon, K.S., Kim, H.J., Kim, K., and Chae, H.Z. (2001). Cyclophilin a binds to peroxiredoxins and activates its peroxidase activity. *J. Biol. Chem.* *276*, 29826-29832.

Lu, Y.J., Wu, C.S., Li, H.P., Liu, H.P., Lu, C.Y., Leu, Y.W., Wang, C.S., Chen, L.C., Lin, K.H., and Chang, Y.S. (2010). Aberrant methylation impairs low density lipoprotein receptor-related protein 1B tumor suppressor function in gastric cancer. *Gene Chromosomes Cancer* *49*, 412-424.

Madjd, Z., Pinder, S.E., Paish, C., Ellis, I.O., Carmichael, J., and Durrant, L.G. (2003). Loss of CD59 expression in breast tumours correlates with poor survival. *J. Pathol.* *200*, 633-639.

Matise, M.P., Auerbach, W., and Joyner, A. (1999). Production of targeted embryonic stem cell clones. In *Gene targeting: a practical approach*, A. Joyner, ed. (Oxford: Oxford University Press), pp. 101-132.

Menuet, C., Cazals, Y., Gestreau, C., Borghgraef, P., Gielis, L., Dutschmann, M., Van Leuven, F., and Hilaire, G. (2011). Age-related impairment of ultrasonic vocalization in Tau.P301L mice: possible implication for progressive language disorders. *PLoS One* *6*, e25770.

Meyer zum Gottesberge, A.M., Felix, H., Reuter, A., and Weiher, H. (2001). Ultrastructural and physiological defects in the cochlea of the Mpv17 mouse strain. A comparison between young and old adult animals. *Hear. Res.* *156*, 69-80.

Michard, Q., Commo, S., Belaidi, J.P., Alleaume, A.M., Michelet, J.F., Daronnat, E., Eilstein, J., Duche, D., Marrot, L., and Bernard, B.A. (2008a). TRP-2 specifically decreases WM35 cell sensitivity to oxidative stress. *Free Radic. Biol. Med.* *44*, 1023-1031.

Michard, Q., Commo, S., Rocchetti, J., El Houari, F., Alleaume, A.M., Wakamatsu, K., Ito, S., and Bernard, B.A. (2008b). TRP-2 expression protects HEK cells from dopamine- and hydroquinone-induced toxicity. *Free Radic. Biol. Med.* *45*, 1002-1010.

Nakagawa, T., Pimkhaokham, A., Suzuki, E., Omura, K., Inazawa, J., and Imoto, I. (2006). Genetic or epigenetic silencing of low density lipoprotein receptor-related protein 1B expression in oral squamous cell carcinoma. *Cancer Sci.* *97*, 1070-1074.

Nicholls, D.G., and Ward, M.W. (2000). Mitochondrial membrane potential and neuronal glutamate excitotoxicity: mortality and millivolts. *Trends Neurosci.* *23*, 166-174.

Roux, I., Hosie, S., Johnson, S.L., Bahloul, A., Cayet, N., Nouaille, S., Kros, C.J., Petit, C., and Safieddine, S. (2009). Myosin VI is required for the proper maturation and function of inner hair cell ribbon synapses. *Hum. Mol. Genet.* *18*, 4615-4628.

Roux, I., Safieddine, S., Nouvian, R., Grati, M., Simmler, M.-C., Bahloul, A., Perfettini, I., Le Gall, M., Rostaing, P., Hamard, G., *et al.* (2006). Otoferlin, defective in a human deafness form, is essential for exocytosis at the auditory ribbon synapse. *Cell* *127*, 277-289.

Schenk, T., Stengel, S., Goellner, S., Steinbach, D., and Saluz, H.P. (2007). Hypomethylation of *PRAME* is responsible for its aberrant overexpression in human malignancies. *Gene Chromosomes Cancer* *46*, 796-804.

Sonoda, I., Imoto, I., Inoue, J., Shibata, T., Shimada, Y., Chin, K., Imamura, M., Amagasa, T., Gray, J.W., Hirohashi, S., *et al.* (2004). Frequent silencing of low density lipoprotein receptor-related protein 1B (LRP1B) expression by genetic and epigenetic mechanisms in esophageal squamous cell carcinoma. *Cancer Res.* *64*, 3741-3747.

Spinazzola, A., Viscomi, C., Fernandez-Vizarra, E., Carrara, F., D'Adamo, P., Calvo, S., Marsano, R.M., Donnini, C., Weiher, H., Strisciuglio, P., *et al.* (2006). *MPV17* encodes an inner mitochondrial membrane protein and is mutated in infantile hepatic mitochondrial DNA depletion. *Nat. Genet.* *38*, 570-575.

Teudt, I.U., and Richter, C.P. (2007). The hemicochlea preparation of the guinea pig and other mammalian cochleae. *J. Neurosci. Methods* *162*, 187-197.

Thelen, N., Breuskin, I., Malgrange, B., and Thiry, M. (2009). Early identification of inner pillar cells during rat cochlear development. *Cell Tissue Res.* *337*, 1-14.

Tu, S., Shin, Y., Zago, W.M., States, B.A., Eroshkin, A., Lipton, S.A., Tong, G.G., and Nakanishi, N. (2007). Takusan: a large gene family that regulates synaptic activity. *Neuron* *55*, 69-85.

Watson, N.F., Durrant, L.G., Madjd, Z., Ellis, I.O., Scholefield, J.H., and Spendlove, I. (2006). Expression of the membrane complement regulatory protein CD59 (protectin) is

associated with reduced survival in colorectal cancer patients. *Cancer Immunol. Immunother.* *55*, 973-980.

Wool, I.G. (1996). Extraribosomal functions of ribosomal proteins. *Trends Biochem. Sci.* *21*, 164-165.

Xu, J. (2005). Preparation, culture, and immortalization of mouse embryonic fibroblasts. In *Current Protocols in Molecular Biology.* *70*, 28.1:28.1.1–28.1.8.

Figure 1

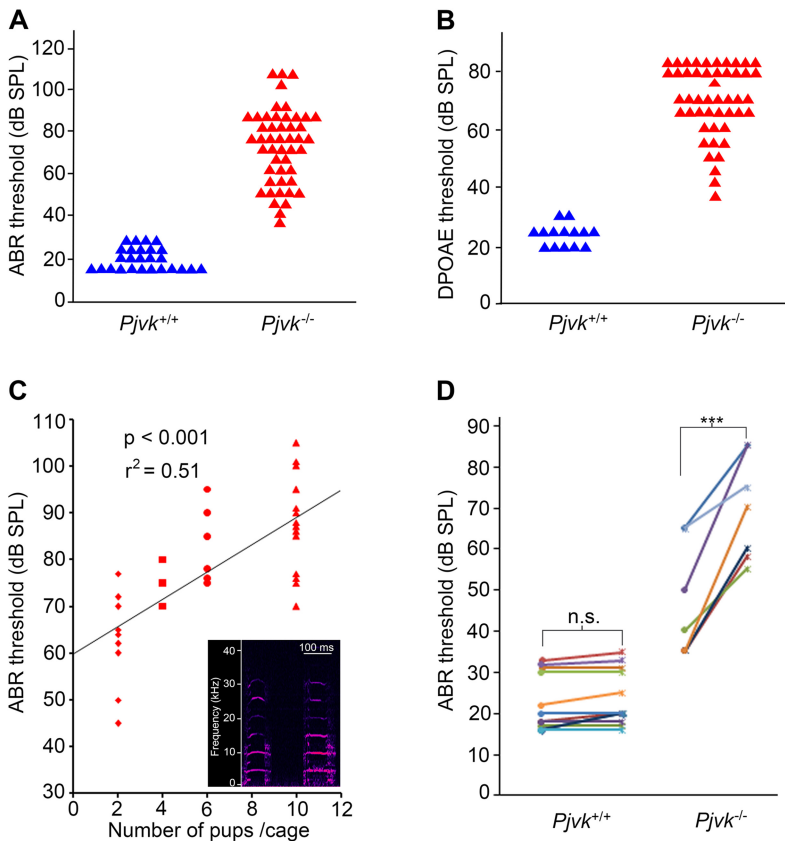


Figure 2

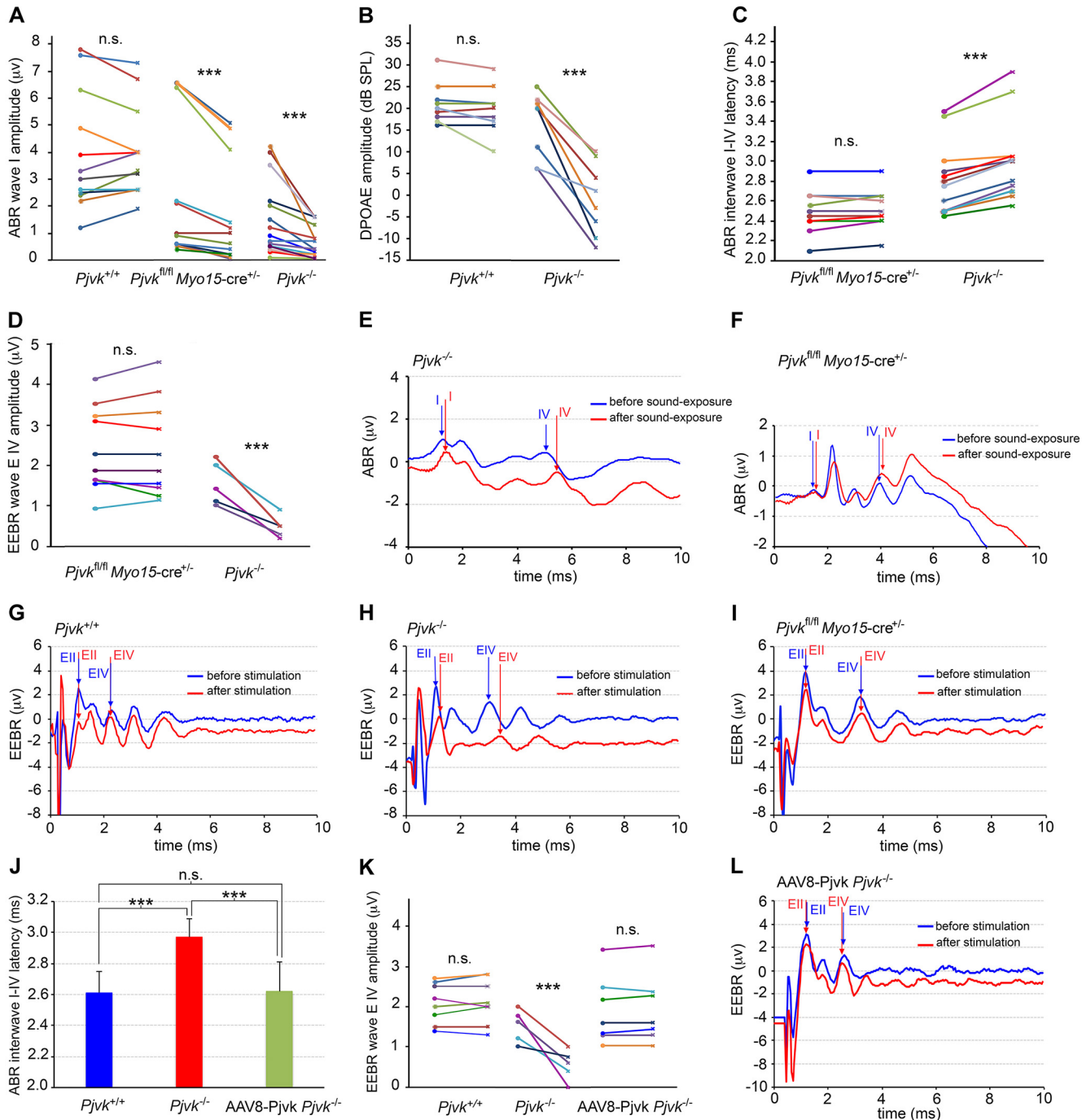


Figure 3

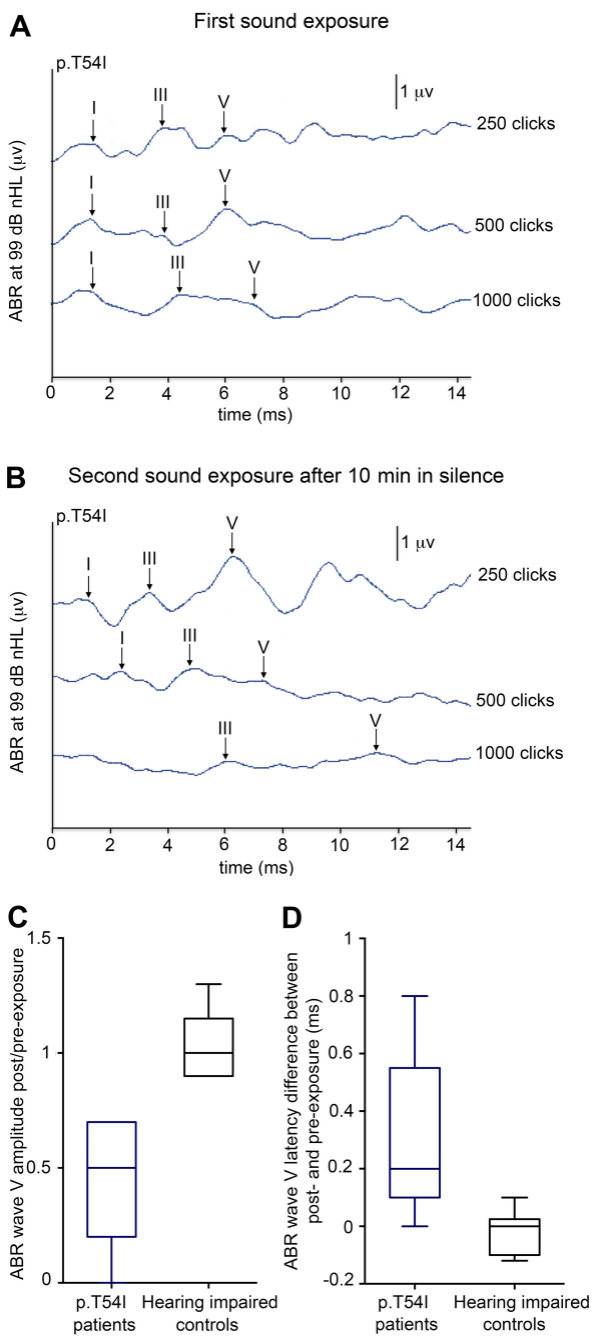
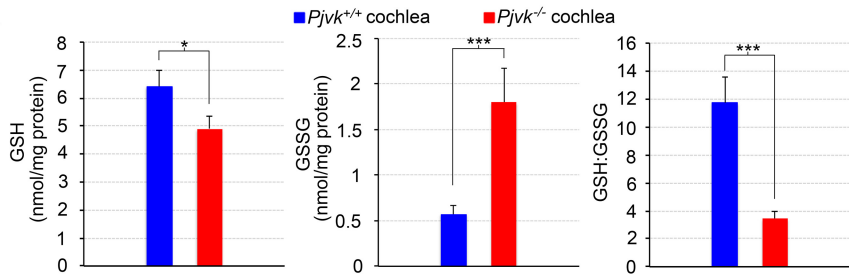


Figure 4

A



B

F-actin / BK- α subunit / DAPI

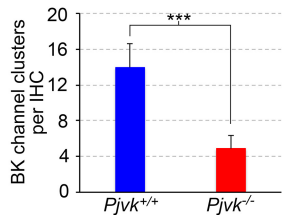
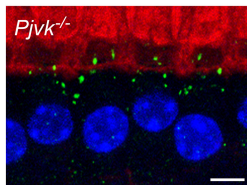
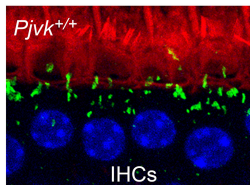
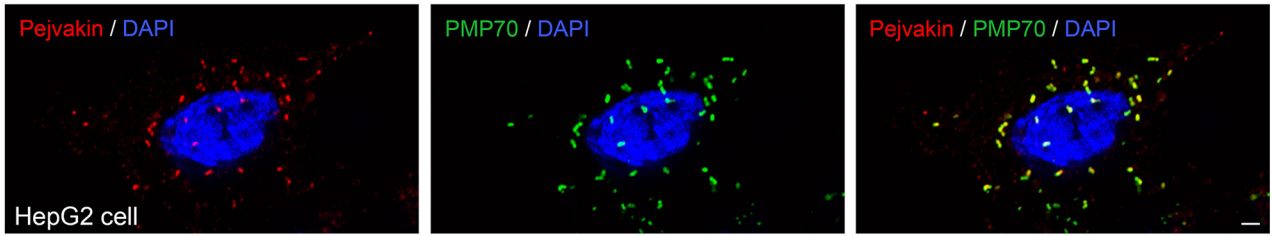
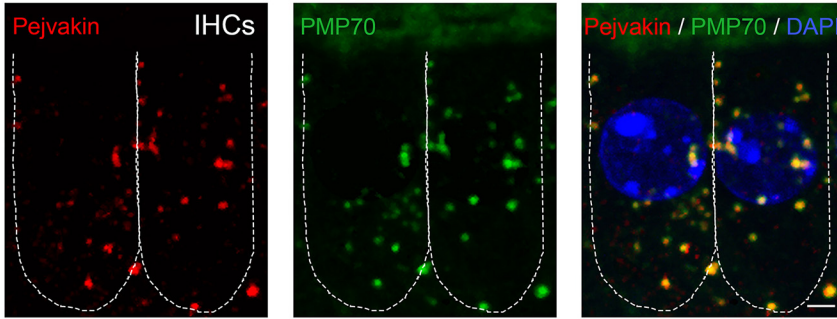


Figure 5

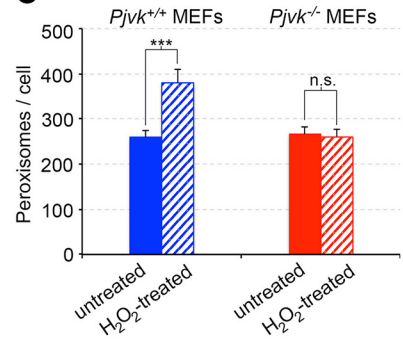
A



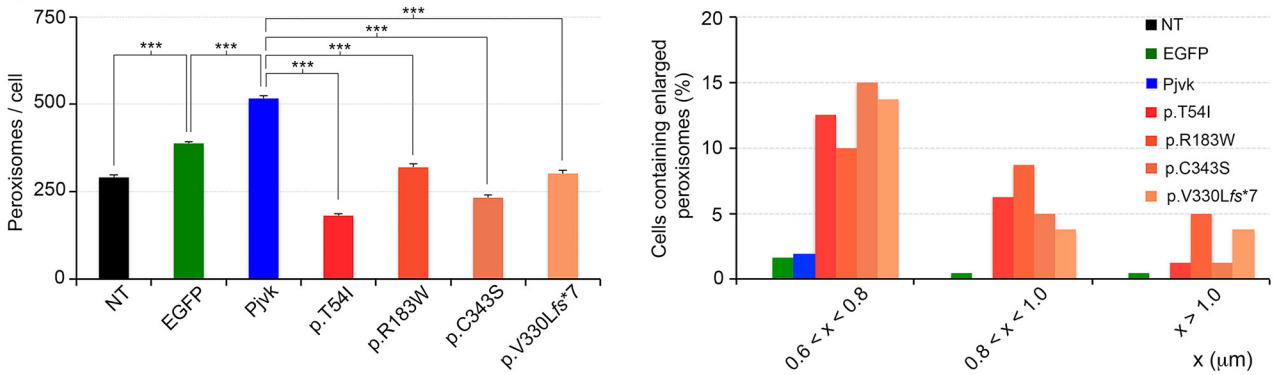
B



C



D



E

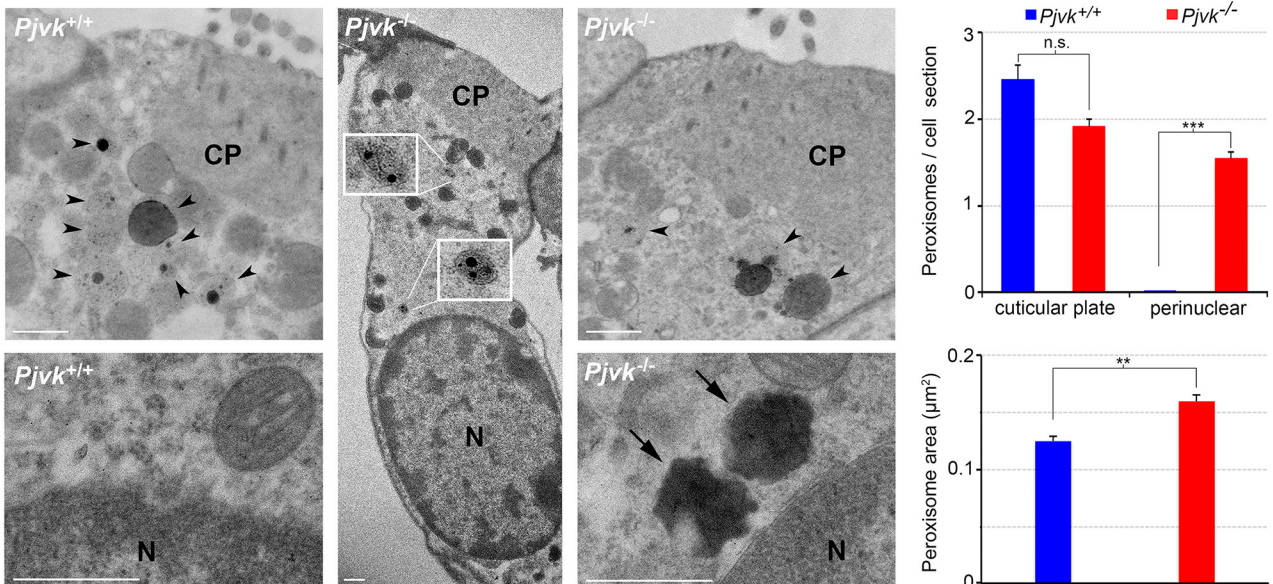


Figure 7

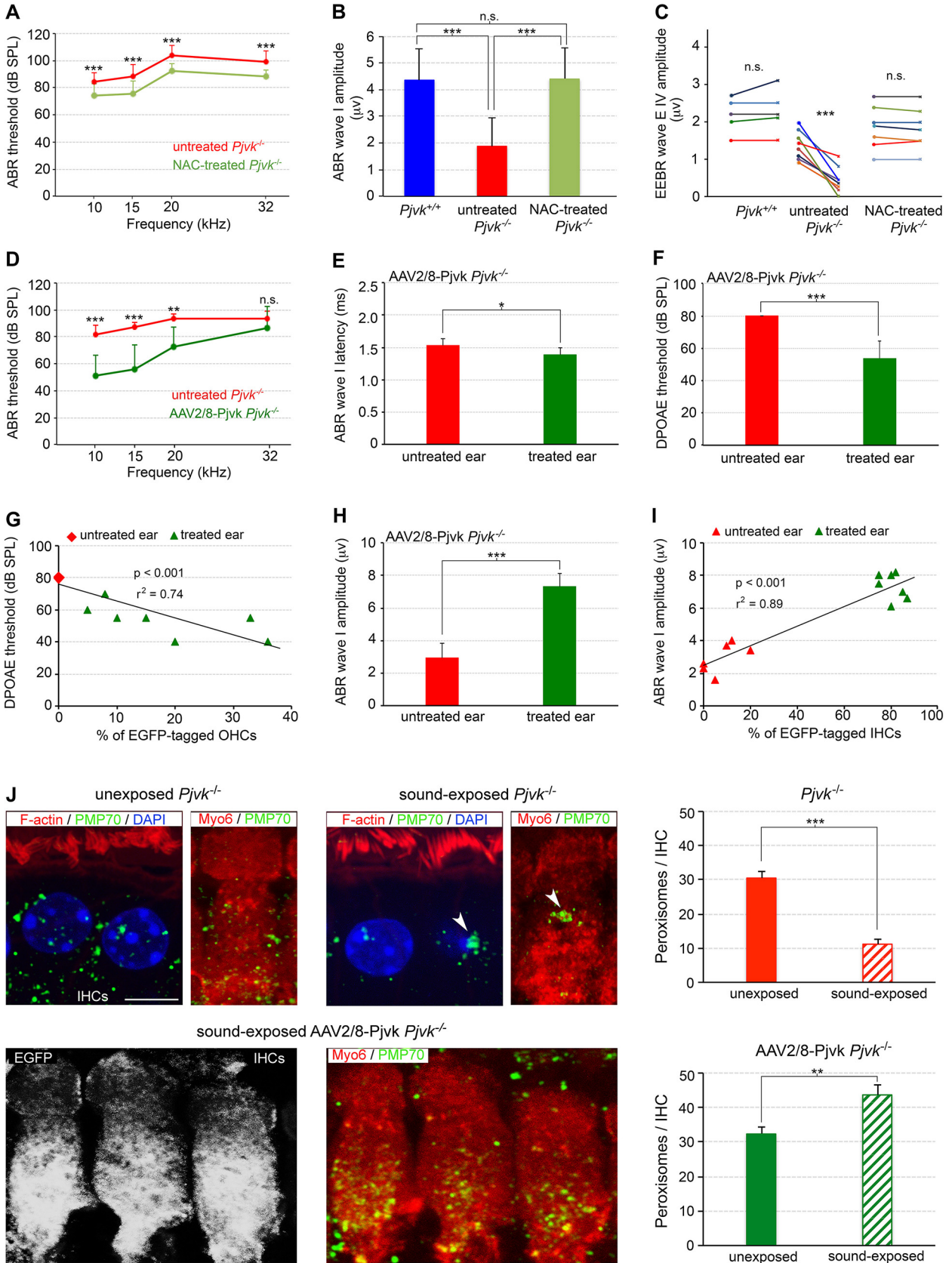


Figure S1

A

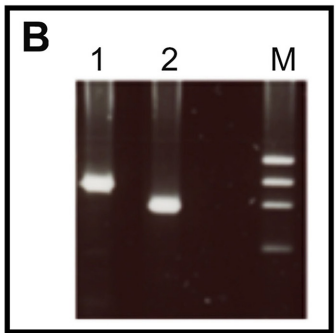
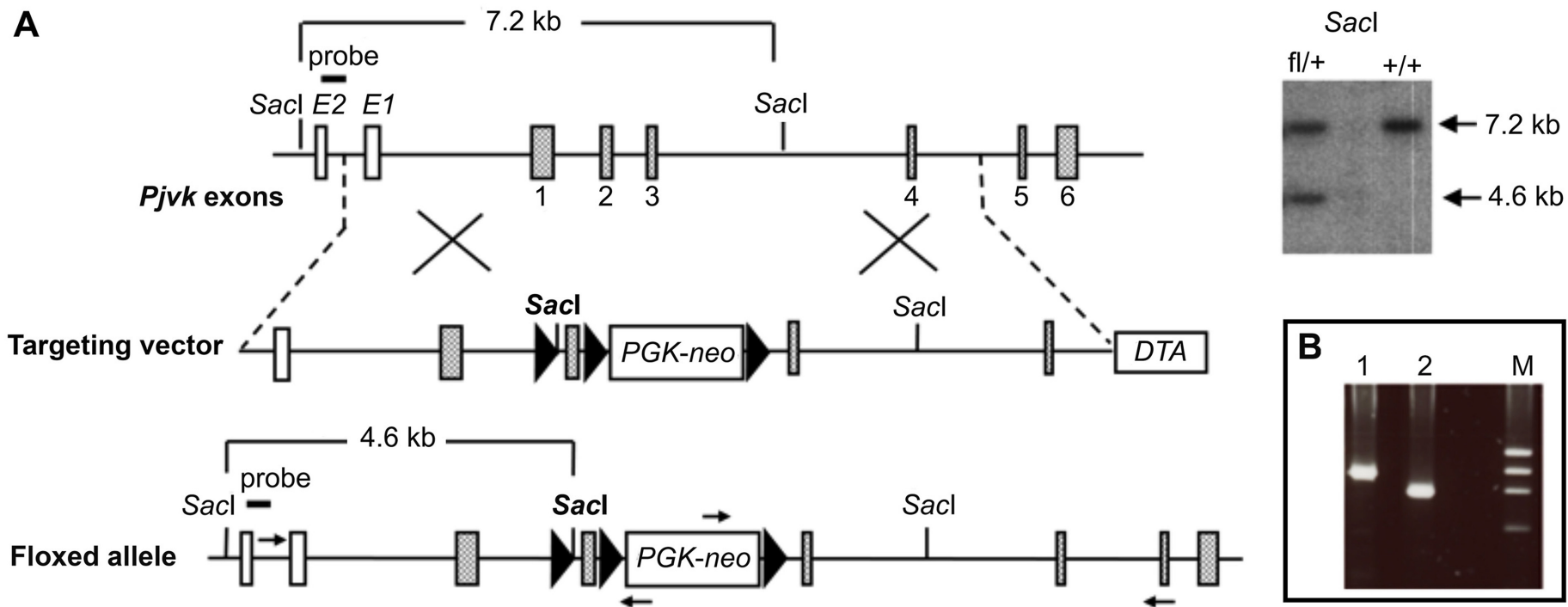


Figure S2

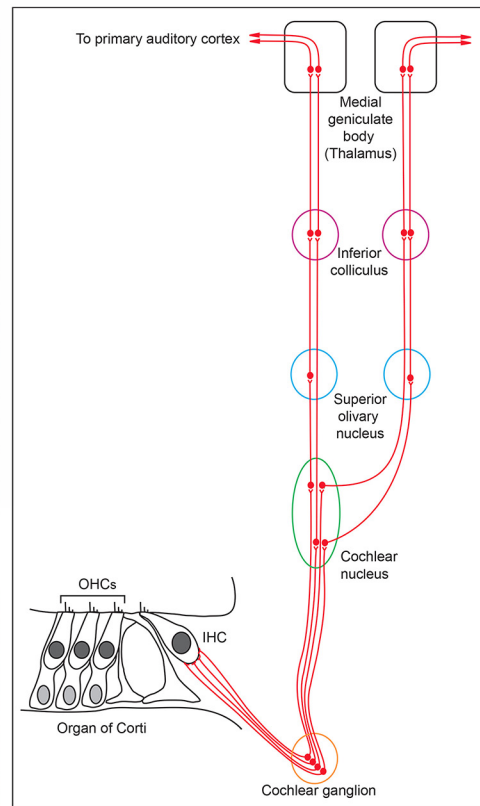
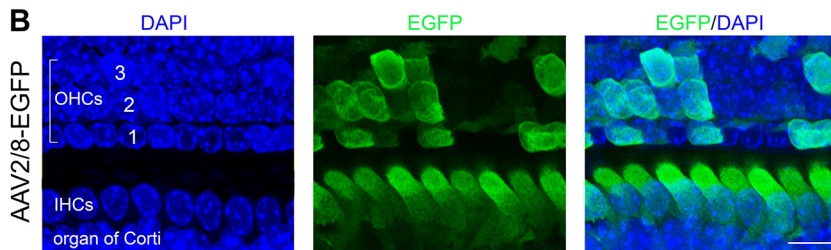
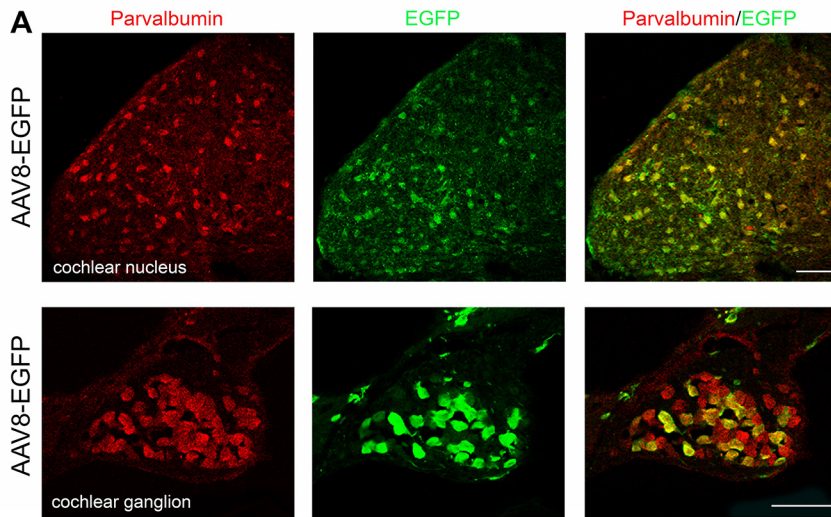


Figure S3

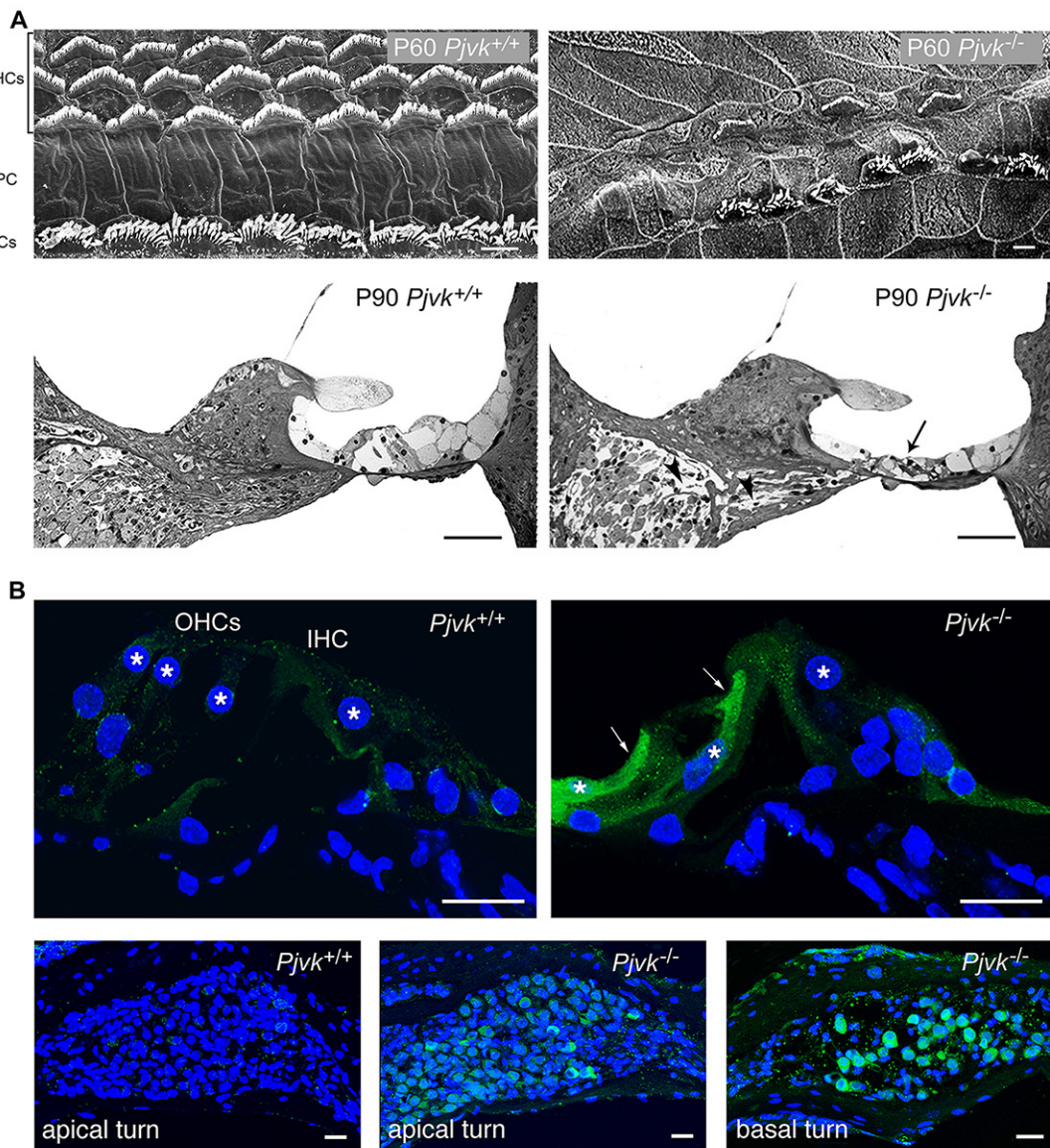


Figure S4

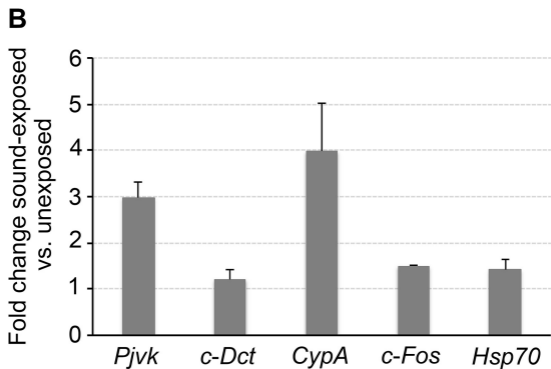
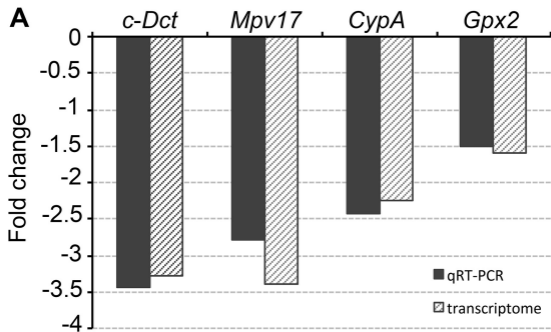


Figure S5

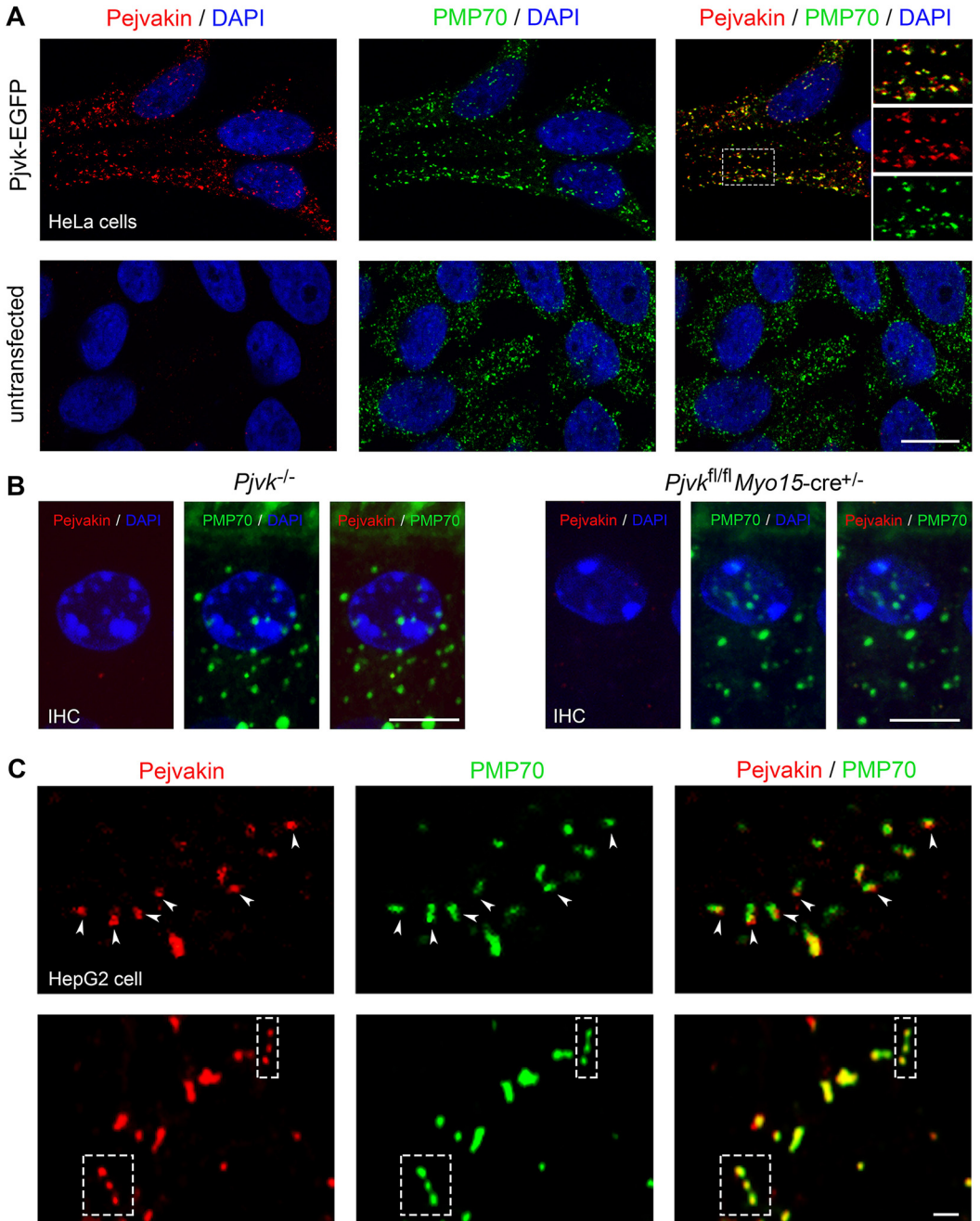
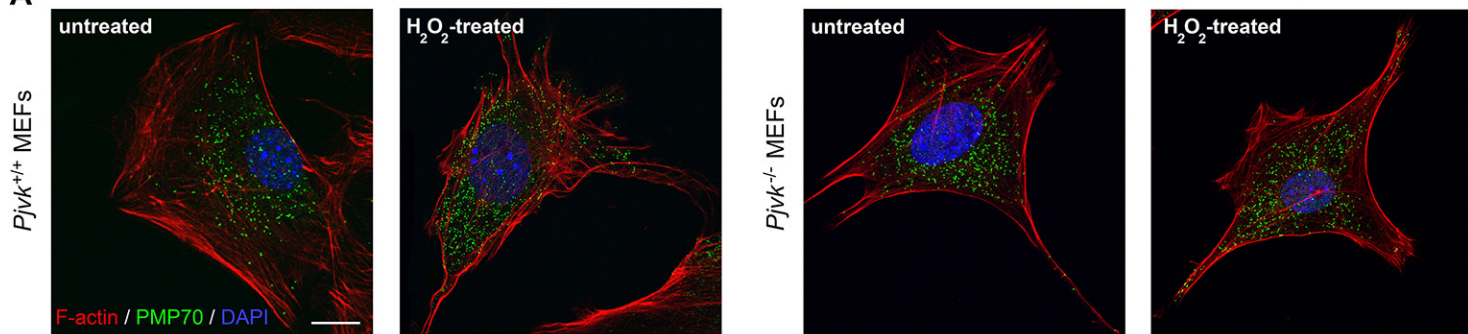


Figure S6

A



B

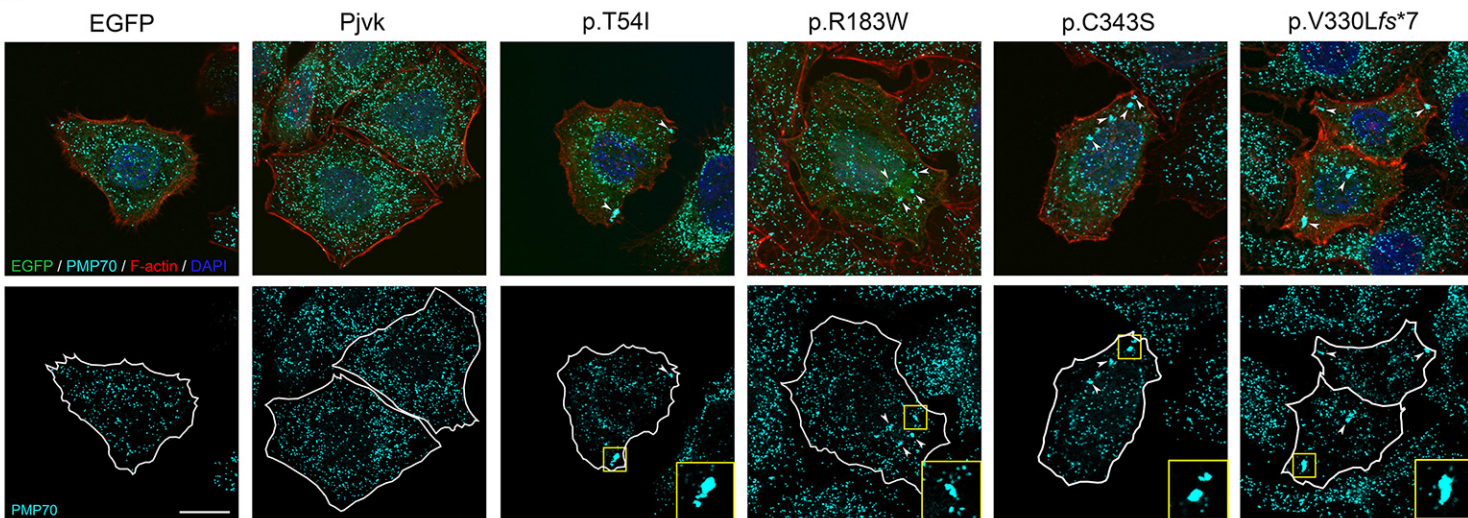


Figure S7

